Ocean Engineering 364 (2026) 126952

Contents lists available at ScienceDirect

Ocean Engineering

journal homepage: www.elsevier.com/locate/oceaneng

Research paper

Motion control of a two-body point absorber wave energy converter for underwater vehicle docking and charging

David Okushemiya [a,b,*], Bryson Robertson [c], Junhui Lou [a,b], Solomon C. Yim [a,b]

[a] Pacific Marine Energy Center, Oregon State University, 97333, OR, USA
[b] Civil and Construction Engineering, Oregon State University, 97333, OR, USA
[c] Mechanical Engineering, University of Victoria, BC, Canada

ARTICLE INFO

Keywords:
Wave energy
Two-body point absorber
Underwater docking
Underwater charging
PTO control
Numerical modeling
Powering the blue economy

ABSTRACT

This study develops and investigates motion control of a two-body point absorber wave energy converter (WEC) to allow for docking and recharge of an unmanned underwater vehicle (UUV). It addresses the conflicting requirements between power-mode operation, which favors large motions for energy extraction, and docking-mode operation, which requires minimal dock motion for UUV docking compatibility. Four control modes are considered: power mode (PM), passive docking mode (DM) with zero PTO damping, and two active strategies: velocity-proportional (VP) and linear quadratic (LQ) control. Results show that PM produces large dock heave velocities on the order of 0.6–1.4 m/s, which are unfavorable for docking, while DM reduces motion but remains insufficient, particularly in moderate to rough sea states. VP control achieves superior motion regulation, reducing dock velocities to below 0.03 m/s, but requires higher reactive power, resulting in negative net power. In contrast, LQ control reduces velocities to 0.07–0.28 m/s while maintaining positive net power, corresponding to a 70%–85% reduction relative to power-mode operation. Performance is fundamentally constrained by the inherent heave-only WEC power-take-off (PTO) actuation, which limits the ability to control surge and pitch, and motivates system-level improvements in controllability. The results establish docking-mode control as a distinct operational framework and provide guidance for integrated WEC–UUV system and control design.

1. Introduction

Unmanned underwater vehicles (UUVs) support a wide range of ocean missions, including observation, monitoring, intervention, and defense activities (Podder et al., 2004; Yazdani et al., 2020; Lin et al., 2022). Their usefulness, however, is heavily constrained by limited onboard energy storage, which restricts mission endurance and often requires repeated recoveries for recharging (Hagen et al., 2008; Liu et al., 2024). This limits their overall persistence, operational endurance, and efficiency (Zeng et al., 2015). Ocean waves offer significant potential for at-sea power generation, through wave energy converters (WECs) (Robertson et al., 2016), positioning WECs as promising platforms for docking and charging UUVs, thereby enabling persistent and longer endurance UUV missions. However, the published literature and functional deployment of WECs to support underwater docking and recharging of UUVs remains largely unexplored.

Floating two-body point absorber WECs are among the most-widely studied WEC archetypes (Jin and Greaves, 2021; Nemoto et al., 2022) and thus offer a practical basis for WEC–UUV system integration. They consist of a surface float and a submerged reacting body, referred to as the spar. The two bodies are connected through a power-take-off (PTO) unit (Beatty et al., 2019). Power is generated from the relative heave motion between the float and spar. In a two-body point absorber WEC–UUV system, the docking station is usually connected to the spar (Okushemiya et al., 2025), so its' motion is defined by the spar response, with the degree of motion transfer depending on whether the dock is rigidly attached or tethered. During power extraction, the float and spar typically undergo significant relative motions (Li et al., 2023), which increases dock motion and reduces docking feasibility (i.e., the chances of successful UUV docking) (Okushemiya et al., 2025, 2026a). This creates conflicting requirements between the power and docking functionalities of WEC–UUV systems. Although real-world docking success depends on navigation, sensing, and communication between UUV and dock (Hasan et al., 2024), a fundamental system requirement is that dock motion remains within the motion limits of the UUV (Okushemiya et al., 2026a). Additionally, when docking near

* Corresponding author.
E-mail address: okushemd@oregonstate.edu (D. Okushemiya).

https://doi.org/10.1016/j.oceaneng.2026.126952
Received 8 May 2026; Received in revised form 27 June 2026; Accepted 6 July 2026
Available online 14 July 2026

the free surface or under large waves, wave-induced forces on the UUV itself will influence docking success (Lou et al., 2025).

These contrasting requirements between power extraction and UUV docking success introduce two operational modes in WEC–UUV systems: a power mode, in which the WEC operates to extract and store energy for UUV recharging; and a docking mode, in which the motion of the docking station operates to remain minimal and compatible for increased chance of successful UUV docking. Operating across these modes requires a control strategy that can adjust the WEC response based on the operational objective. While numerous control strategies have been developed for maximizing wave power extraction (Coe et al., 2017), limited attention has been given to control approaches that enable 'docking mode operation' - by ensuring that dock motions remain minimal and compatible with UUV motions for high docking feasibility.

This study develops and tests motion-control strategies for floating point absorber WECs to enable successful UUV docking. The central research question addresses how the dock motion can be controlled to remain minimal and compatible with UUV motions for improved chances of successful UUV docking.

2. Background

2.1. Wave energy powered UUV missions

Reliable access to energy remains a key requirement for extending the operational duration and persistence of UUV missions. Ocean waves offer a substantial and largely underutilized energy resource that can be harnessed to generate electrical power for UUV recharging (Zeng and Wang, 2023; Liu et al., 2024; Department of Energy, 2019). One proposed approach is to embed wave energy harvesting capabilities directly within the UUV through an onboard power take-off system, thus enabling autonomous energy extraction without reliance on external infrastructure (Li et al., 2022; Zhang et al., 2023, 2024; Mundon et al., 2024). However, the relatively small size of UUVs compared to ocean wavelengths limits the efficiency of this approach and results in low power capture (Zhang et al., 2024). Alternatively, standalone wave energy converters provide a more effective means of harvesting wave energy due to their larger scale and improved hydrodynamic interaction with waves. This configuration introduces the need for reliable docking and charging systems to support autonomous UUV operations (Driscol et al., 2021; Chen et al., 2024; Okushemiya et al., 2025, 2026a; Rusch et al., 2026).

Comparing UUV-integrated energy harvesters and standalone WEC systems, the latter are considered in this study as their size relative to ocean wavelengths allows for more efficient wave energy capture. Standalone WECs appear in several archetypes, each employing different physical mechanisms to capture wave energy, including terminators, attenuators, oscillating-body devices, and point absorbers (Jin and Greaves, 2021; Robertson et al., 2021a). Among these archetypes, point absorber WECs are among the most widely studied because they can exploit more energetic waves and absorb energy from all wave directions (Nemoto et al., 2022). Several small-sized floating point absorbers suitable for WEC–UUV integration have been developed and experimentally tested and validated. Beatty et al. (2019) reported model-scale experiments of two self-reacting point absorber WECs tested at a 1:25 geometric scale using a 0.6 m float diameter model, corresponding to a full-scale diameter of 15 m. The first device, denoted WEC A, was based on the WaveBob™ concept and produced an average full-scale power of 52 kW, while WEC B, modeled after the PowerBuoy®, produced 73 kW. Using Froude scaling for power ($P \propto \lambda^{3.5}$), a consistent 1:3 scale representation of these devices would have a float diameter of 5 m and yield full-scale equivalent power of approximately 1.11 kW for WEC A and 1.56 kW for WEC B. Other experimental studies on similar floating point absorber WECs examining survivability, hydrodynamic response, and power absorption have been reported in Xu et al. (2019), Wu et al. (2021), Rahimi et al. (2022), Li et al. (2023), Beringer et al. (2025). The power absorption reported in these studies can inform assessments of UUV recharging capability in WEC–UUV system integration; however, they do not address whether the associated device motions are compatible with the motion limits required for increased chance successful UUV docking.

2.2. Underwater docking systems

Aside from wave energy powered UUV concepts, independent research and development has been ongoing on underwater docking technology, with Yazdani et al. (2020), Liu et al. (2024) providing a recent review. Early developments can be traced to the REMUS docking system introduced in 1997 (Stokey et al., 1997, 2001). The advancement of underwater docking systems aimed to extend operational duration, persistence, and mission efficiency. This is particularly relevant for resident UUVs (Song et al., 2020) where an underwater dock can provide a stable and dependable platform for charging when and if a reliable source of energy supply is available. Underwater docking systems developed in the literature generally fall into two broad categories: seafloor mounted and suspended docking systems (Lin et al., 2022; Liu et al., 2024). Seafloor mounted docking systems represented the earliest direction in underwater docking technology (Stokey et al., 1997, 2001). In this configuration, the dock is rigidly fixed to the seabed and connected to a power source usually on the sea surface through subsea cables, providing a highly stable platform for reliable UUV docking with minimal influence from ocean waves. However, their practicality has declined (Lin et al., 2022) due to several limitations. Deep deployments require UUVs to descend long distances before recharging, consuming significant time and energy, while long power and communication cables increase system cost and reduce power-transfer efficiency. In addition, uneven or soft seabed conditions can complicate installation and long-term stability of the dock (Guo et al., 2024a). Recent years have seen growing interest in suspended underwater docking systems (Lin et al., 2022; Guo et al., 2024b). In these configurations, the docking station is attached to a tether, with the opposite end connected either to a surface float Fletcher et al. (2017), Sarda and Dhanak (2019), Lin et al. (2022), Meng et al. (2019) or to a seafloor anchor (Guo et al., 2024b,a; Zheng et al., 2024). Suspended docks enable docking at more accessible depths, reduce the energy a UUV must expend to locate and reach the station, and require shorter power and communication cables, which lowers cabling cost and improves power-transfer efficiency. Configurations supported by a surface float closely resemble the arrangement expected for WEC–UUV systems, where the dock would likewise be suspended beneath a surface body. These advantages indicate promising future applications for suspended docking concepts (Guo et al., 2024b).

2.3. WEC–UUV system integration

Research on integrated WEC–UUV systems remains in its early stages, but existing underwater docking and charging concepts have naturally informed the configurations proposed for WEC–UUV system integration. Okushemiya et al. (2025) identified three representative configurations: seafloor-mounted, rigid-mounted, and tethered docks. In the seafloor-mounted configuration, the docking station is rigidly fixed to the seabed and connected to the WEC on the surface via a cable/tether. In the rigid-mounted configuration, the dock is rigidly attached to the WEC structure and therefore fully inherits the WEC's motion response. In the tethered configuration, the dock is connected to the WEC via a flexible tether, allowing partial motion independence while remaining mechanically linked to the WEC. While seafloor-mounted docks offer a stationary platform, recent advances in underwater docking technology have shifted toward suspended docking systems (Lin et al., 2022; Guo et al., 2024b). As a result, tethered and rigid-mounted configurations represent promising candidates for advancing WEC–UUV system integration.

As introduced in Section 1, WEC–UUV systems require that the motion of the docking station remain minimal and within the UUV's allowable motion limits to improve the chances of successful docking. This requirement generally conflicts with the power-generation behavior of floating point absorbers, which exhibit large relative motions during power extraction (de Andrés et al., 2013; Li et al., 2023). Addressing this conflict requires control strategies that adjust the WEC response between power and docking modes.

2.4. Review of WEC control strategies

Control strategies for WECs have traditionally focused on maximizing power absorption, wherein the WEC body dynamic response is tuned to achieve resonance by controlling the body's velocity to align in phase with the wave excitation force (Coe et al., 2017). Numerous control approaches have been developed to achieve this objective, and most fall under broad categories in the WEC literature, including resistive control, complex conjugate (CC) control, model predictive control (MPC), dynamic programming (DP), shape-based control, linear-quadratic (LQ) control, proportional–derivative variants of conjugate control, and latching control (Coe et al., 2017; Bacelli, 2014).

Resistive control applies a velocity-proportional damping force through the PTO, where an optimal damping coefficient, or force, is selected to maximize power absorption. Analytical formulations for this optimal damping have been developed by Falnes and Kurniawan (2020) for regular waves and by Zou et al. (2017) for irregular seas. In a two-body point absorber WEC–UUV system, this resistive PTO damping may provide a passive means of controlling spar motion. Increasing the PTO damping toward, and beyond, its optimal value will increase the coupling between the float and spar, causing the spar to experience larger motions driven by the float's wave-induced motion. Conversely, setting the PTO damping to zero allows the spar to move more independently from the float, potentially reducing spar motion. With the dock attached to the spar, these behaviors suggest that resistive control could, in principle, support passive docking mode control.

Complex conjugate (CC) control seeks to maximize absorbed power by matching the PTO impedance to the complex conjugate of the WEC's intrinsic hydrodynamic impedance (Falnes and Kurniawan, 2020; Coe et al., 2021b). This results in an acausal control system, requiring future knowledge of the wave excitation, which limits practical implementation in the absence of accurate wave prediction (Coe et al., 2017). The proportional–derivative (PD) variants of conjugate control offer a practical means of overcoming CC control acausality. Coe et al. (2021b) exploited the narrow-band nature of ocean waves to approximate the complex-conjugate PTO impedance over the limited frequency range containing most of the wave energy. This was achieved by tuning the gains of a proportional–integral–derivative (PID) controller so that its frequency response approximated the desired impedance within the dominant frequencies of each time-varying sea state (Forbush et al., 2020). More advanced forms, such as multi-resonant PD implementations, tune individual gains for each of the wave frequency components to further improve power capture (Song et al., 2016; Abdelkhalik and Zou, 2019). Since conjugate control strategies are intrinsically motion amplifying owing to the resonance achieved through impedance matching, they do not appear suited for adaptation to docking mode control.

Model predictive control (MPC) and linear quadratic (LQ) control are feedback-based strategies that apply a PTO control law to shape the WEC dynamic response toward a desired objective (Åström and Murray, 2021). Both are optimization-based approaches in which the PTO control force is selected to satisfy an objective function (Coe et al., 2017). Their use in the WEC literature has focused on maximizing the energy produced by the PTO. MPC achieves this by computing an optimal PTO force over a receding prediction horizon (Zhan et al., 2020; M. Zhang et al., 2024; Gao et al., 2025). LQ control accomplishes the same objective by deriving a state-feedback law that minimizes a quadratic cost function through the solution of a Riccati equation (Scruggs et al., 2013; Kassem et al., 2015; Zou and Abdelkhalik, 2020). For a two-body point absorber WEC, these feedback control (MPC and LQ) framework could, in principle, be adapted for docking mode control by redefining the optimization objective to minimize spar motion, which the dock is attached to, rather than maximize energy capture.

Dynamic programming (DP) and shape-based (SB) control have also been explored for WEC power control, but both present fundamental limitations that complicate their adaptation for docking mode control. DP is computationally intensive, difficult to implement in real time, and lacks a standard mathematical formulation, requiring a new tailored algorithm for each specific application (Coe et al., 2017). SB control relies on several initialization parameters that are highly sensitive to the sea state, adding configuration complexity and often leading to suboptimal performance (Coe et al., 2017).

Latching control is a switching strategy in which the WEC is held nearly fixed ("latched") and released to shift its effective resonance period and maximize power absorption (Korde, 2002). In the latched state, the PTO behaves as a very large resistive damping; for a two-body point absorber this effectively locks the bodies together, transferring larger wave-induced float motions to the spar. As such, latching control does not offer a viable avenue for adaptation to docking mode control.

Across the reviewed control strategies, existing WEC controllers are fundamentally designed to amplify or strategically exploit device motion to maximize power absorption. This objective directly conflicts with docking mode control requirements, which requires minimal dock motion to maintain compatibility with UUV motion limits. Although some control strategies contain theoretical elements that could, in principle, be adapted for the docking mode control (e.g., resistive control with zero damping or feedback controllers with modified objective functions for UUV docking), no prior study has formulated or evaluated a control framework explicitly aimed at docking mode operation. This gap motivates the present study, which investigates control strategies for achieving compatible dock motion required for increased chance of successful UUV docking in floating point absorber WEC–UUV systems.

3. Case study: WEC-UUV system

A WEC–UUV system consists of the WEC, the UUV, and a docking station that interfaces the WEC and UUV providing a medium for docking, power storage and transfer, and data transfer. Together, these components interact within the environment of a representative ocean site to enable resident and persistent UUV operations.

3.1. WEC

The case study WEC considered in this work is the Laboratory Upgrade Point Absorber (LUPA), an open-source point absorber designed, tested, and validated by Beringer et al. (2025). It is a two-body point absorber WEC consisting of a buoyant surface float and a reactionary spar equipped with a heave plate, as shown in Fig. 1.

LUPA was originally designed, tested, and validated at laboratory scale with a float diameter of 1 m (Beringer et al., 2025). In this study, the WEC geometry is uniformly scaled by a factor of three relative to the laboratory model, corresponding to a 3:1 geometric scale shown in Fig. 1. This scale is representative of small, low-power utility WECs intended for low-energy applications such as UUV docking and recharging, for which large-scale power generation is not required. For this study, the environmental conditions are assumed to be representative of PacWave south test site with about 70 m water depth (Freeman et al., 2022; Robertson et al., 2021b).

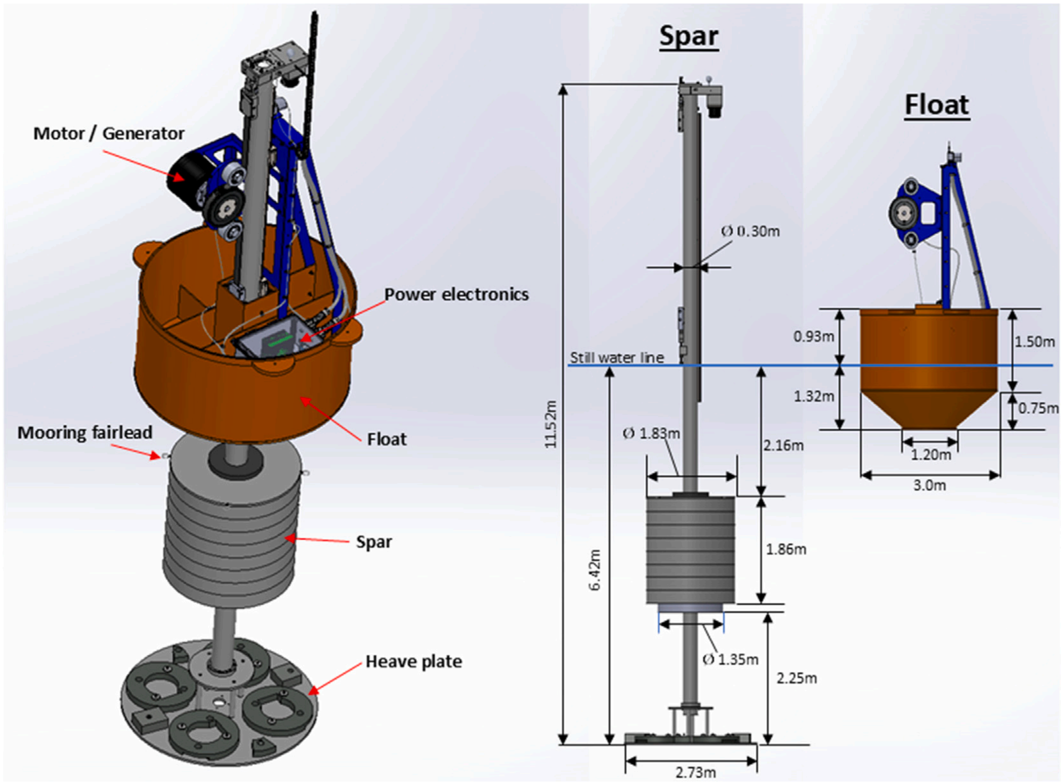

Fig. 1. Schematics and description of LUPA WEC.

Table 1
Mass and inertia properties of the LUPA WEC scaled by a factor of three, relative to the still water line reference frame.

Component	Mass (kg)	Cg_x (m)	Cg_y (m)	Cg_z (m)	I_{xx} (kg m^2)	I_{yy} (kg m^2)	I_{zz} (kg m^2)
Float	6637.68	−0.03	0.03	0.06	15 600	16 071	4163
Spar	5459.67	−0.03	0.00	−4.35	74 083	74 175	3810

The main geometric and physical properties of the scaled WEC used in this study are listed in Table 1 given with reference to the still water line (as shown in Fig. 1). Primary modification to the original WEC configuration in model was the addition of buoyancy to spar to compensate for the weight of the docking station and docked UUV, while detailed structural integration considerations are beyond the scope of this study.

3.2. UUV & docking station

The docking station is modeled to support BlueROV2 in its Heavy configuration (Fig. 2). It was designed and fabricated at Oregon State University to support laboratory-scale docking experiments of the BlueROV2 Heavy UUV in the O.H. Hinsdale Wave Laboratory. The station was originally developed to enable controlled evaluation of UUV docking performance under prescribed motions representative of an oscillating WEC in the wave tank.

The docking station is shown in Fig. 3, it consists of a welded aluminum frame constructed from 1.5 in × 1 in square aluminum tubing. The main docking frame has overall dimensions of 1.00 m in width, 0.83 m in height, and 0.86 m in length, with a total mass of 65.6 kg, including onboard electronics, wireless charging components, and docking hardware.

As shown in Fig. 3, the docking station incorporates an actuation superstructure and gimbal assembly that provide a mechanical interface to an external actuator. This interface was used in wave tank experiments to impose prescribed motions representative of an oscillating WEC; however, these actuation components are not directly modeled in the present numerical study and are shown here for completeness

Fig. 2. BlueROV2 UUV (BlueRobotics, 2023).

4. WEC–UUV motion control modeling framework

The motion control framework for WEC–UUV docking mode adopted is based on a feedback control architecture, as illustrated in Fig. 4. The framework consists of two primary blocks: the WEC–UUV system and the controller.

The WEC–UUV subsystem represents the dynamic plant of interest and may be realized as a numerical model, a physical system, or a combination of both. In the present study, the plant is implemented numerically using the time-domain formulation described in Section 4.1. This numerical representation provides direct access to the system

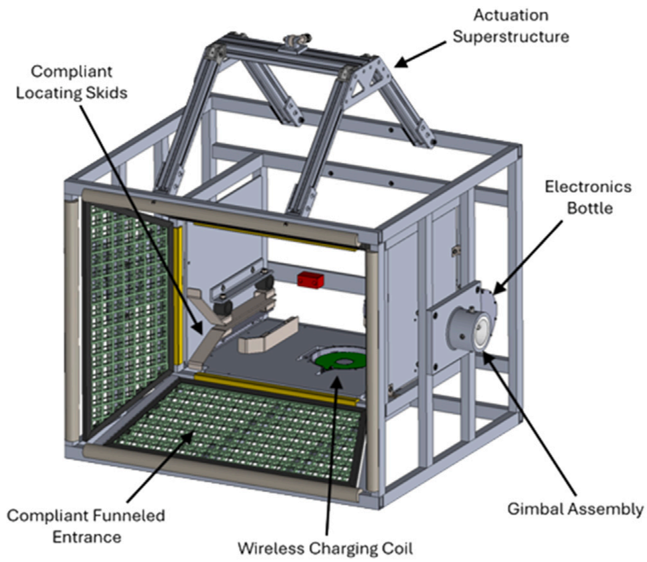

Fig. 3. BlueROV2 UUV docking station.

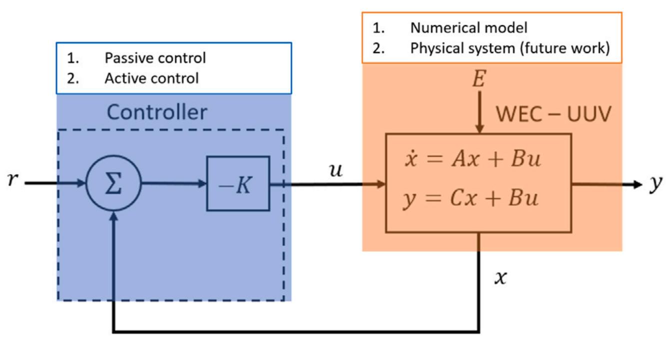

Fig. 4. Modeling framework for WEC-UUV motion control.

states, hydrodynamic responses, and wave excitation inputs, enabling preliminary development, evaluation, and understanding of docking-mode motion control strategies. In contrast, a physical implementation would rely on measured outputs, state estimation, and excitation force estimation. While a physical system introduces sensing uncertainty and additional implementation constraints, the numerical framework enables preliminary assessment and validation of the developed motion control strategies prior to physical implementation. Thus the focus of this work is the development of the numerical framework, and the extension to a physical WEC–UUV platform is identified as future work.

The controller block consists of the control law that computes the actuation force required to regulate dock motion within acceptable limits for UUV docking. The controllers considered in this study are classified as either passive or active, as detailed in Section 5.

Within the feedback control loop, the reference signal r defines the desired docking condition, typically corresponding to minimal relative dock motion. The system state is denoted by x, and the system output (spar/dock velocity) is denoted by y, representing the regulated dock motion variable of interest. The controller computes the control input u based on the deviation between the reference r and the output y. For the two-body point absorber configuration considered here, the control input, u is applied through the PTO actuator and acts on the relative heave motion between the float and the spar. Through this actuation, the control input drives the system output y toward the desired reference motion, r, in the presence of external wave excitation on the WEC-UUV.

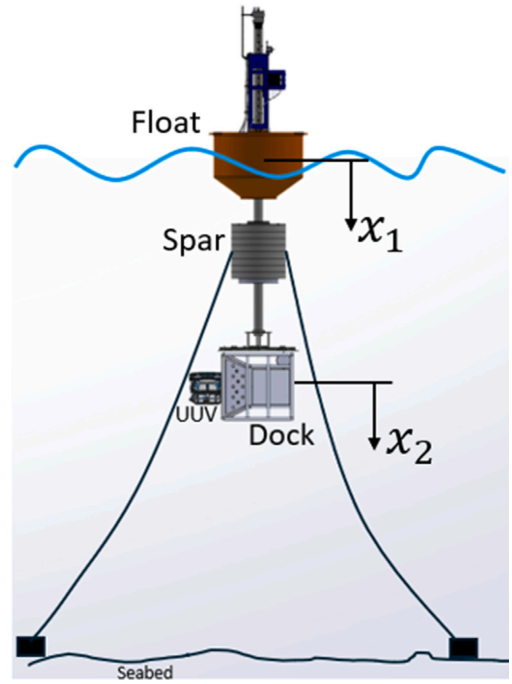

Fig. 5. Schematics of LUPA rigid–mounted dock WEC–UUV system.

4.1. WEC-SIM numerical model of a two-body point absorber WEC–UUV system

The WEC–UUV system analyzed in this study consists of a rigid-mounted dock integrated with the LUPA two-body point absorber wave energy converter, as shown in Fig. 5. The hydrodynamic model of the LUPA WEC implemented in WEC-Sim has been previously validated by Beringer et al. (2025). The upper body (Body 1) corresponds to the surface float, while the lower body (Body 2) comprises the spar with the docking station rigidly attached and treated as a single hydrodynamic body.

The docking structure is mostly composed of slender member elements forming an open-frame geometry as shown in Fig. 3. As a result, its contribution to the potential-flow hydrodynamic coefficients is assumed to be negligible, although its contribution to the viscous drag term is accounted for.

The generalized motion of the float is denoted by x_1, while the motion of the spar–dock rigid assembly is denoted by x_2, where each vector represents the six degree of freedom rigid-body motions (surge, sway, heave, roll, pitch and yaw) of the corresponding body. The two bodies are dynamically coupled via a translational PTO connection.

The numerical model used in this study is based on the time-domain model equation written as:

$$M\ddot{x}(t) = F_{exc}(t) + F_{rad}(t) + F_{hs}(t) + F_{vis}(t) + F_{PTO}(t) \tag{1}$$

where $\ddot{x}(t)$ is the vector of translational and rotational accelerations of the device and M is the rigid-body mass matrix.

$F_{exc}(t)$ is the wave excitation force computed directly in the time domain from a spectral representation of the incident wave field. For a unidirectional irregular wave, it is expressed as

$$F_{exc}(t) = \Re\left[\sum_{i=1}^{N} F_{exc}(\omega_i, \theta)\, e^{i(\omega_i t + \phi_i)} \sqrt{2S(\omega_i)\Delta\omega}\right], \tag{2}$$

where N is the number of discrete frequency components used to represent the wave spectrum, $F_{exc}(\omega_i, \theta)$ is the frequency-dependent complex excitation force coefficient obtained from a boundary-element solver such as WAMIT (WAMIT), θ is the wave heading angle relative to the body, ϕ_i is a uniformly distributed random phase used to realize the irregular wave field, $S(\omega_i)$ is the wave spectral density evaluated at frequency ω_i from a standard wave spectral formulation, and $\Delta\omega$ is the frequency discretization.

The excitation force coefficient $F_{exc}(\omega, \theta)$ is complex-valued and may be written as

$$F_{exc}(\omega, \theta) = |F_{exc}(\omega, \theta)| e^{i\psi(\omega)}, \tag{3}$$

where $\psi(\omega)$ represents the hydrodynamic phase of the excitation force relative to the incident wave.

$F_{rad}(t)$ is the radiation force accounting for fluid memory effects and is expressed as

$$F_{rad}(t) = -A_{\infty}\ddot{x}(t) - \int_0^t K_r(t-\tau)\,\dot{x}(\tau)\,\mathrm{d}\tau, \tag{4}$$

where A_{∞} is the added mass at infinite frequency and $K_r(t)$ is the radiation impulse response function defined as

$$K_r(t) = \frac{2}{\pi}\int_0^{\infty} b(\omega)\cos(\omega t)\,\mathrm{d}\omega, \tag{5}$$

with $b(\omega)$ denoting the frequency-dependent radiation damping coefficients computed using WAMIT.

$F_{hs}(t)$ is the hydrostatic restoring force given by

$$F_{hs}(t) = -K_{hs}\,x(t), \tag{6}$$

where K_{hs} is the hydrostatic restoring stiffness also provided by the BEM solver WAMIT.

$F_{vis}(t)$ is the viscous drag force incorporated using a quadratic Morison-type formulation,

$$F_{vis}(t) = \frac{1}{2}\rho C_d A_p \left(\dot{x}(t) - \dot{x}_f(t)\right)\left|\dot{x}(t) - \dot{x}_f(t)\right|, \tag{7}$$

where ρ is the fluid density, C_d is the drag coefficient, A_p is the projected area normal to the flow direction, and $\dot{x}_f(t)$ is the fluid particle velocity. The values of C_d and A_p are taken from the LUPA validated WEC-SIM model (Beringer et al., 2025). The projected area A_p is scaled to the present geometry and includes the projected area of the dock structure.

The horizontal and vertical fluid particle velocities, denoted as u_f and w_f, respectively, are obtained from linear wave theory as components of the fluid velocity vector $\dot{x}_f$,

$$u_f(x, z, t) = \sum_{i=1}^{N} a_i\omega_i \frac{\cosh\left(k_i(z+h)\right)}{\sinh(k_i h)}\cos(\omega_i t - k_i x + \phi_i), \tag{8}$$

$$w_f(x, z, t) = \sum_{i=1}^{N} a_i\omega_i \frac{\sinh\left(k_i(z+h)\right)}{\sinh(k_i h)}\sin(\omega_i t - k_i x + \phi_i), \tag{9}$$

where z is the vertical coordinate along the water column, measured from the still water level (positive upward), k_i is the wave number gotten from the wave dispersion relationship, and h is the water depth. a_i is the amplitude of each wave component given as;

$$a_i = \sqrt{2S(\omega_i)\Delta\omega}, \tag{10}$$

The PTO force, F_{PTO} is applied equal and opposite on the two bodies through the PTO motor/generator and, for a two-body point absorber, acts along the heave axis based on the relative heave motion between the bodies. In power mode operation, it is defined as

$$F_{PTO} = -C_{PTO}\,\dot{x}_r, \tag{11}$$

where C_{PTO} is the optimal damping coefficient for power mode, and $\dot{x}_r$ corresponds to the relative heave velocity between the two bodies given by

$$\dot{x}_r = \dot{x}_2 - \dot{x}_1, \tag{12}$$

The numerical formulations described above are implemented in WEC-Sim, an open-source time-domain hydrodynamic solver for WECs (Ruehl et al., 2025). The hydrodynamic coefficients are provided in Appendix. Mooring effects are neglected in the present study, and the system is analyzed under freely floating conditions. This assumption allows isolation of the influence of the developed docking-mode control strategies and PTO actuation on spar/dock motion without additional constraints introduced by mooring forces.

5. Docking-mode control strategies

The docking-mode control framework adopted in this study is shown in Fig. 6. In docking mode, the objective shifts from power absorption to regulation of spar/dock motion under wave excitation. Two strategies are considered: passive and active. Passive control modifies the PTO damping without introducing external control effort, relying solely on the inherent hydrodynamic response of the system. However, as wave excitation increases in more energetic sea states, passive control alone may be insufficient to maintain acceptable docking conditions. Active control, in contrast, applies a feedback-generated PTO force, supplying power (reactive power) into the PTO motor/generator that generates a control force to directly regulate the spar/dock responses to satisfy UUV docking feasibility requirements. The two approaches are detailed in the following subsections.

5.1. Passive docking-mode control

The passive docking-mode configuration is implemented by switching the PTO damping coefficient, C_{PTO} in the PTO force (Eq. (11)) as follows;

$$C_{PTO} = \begin{cases} 0, & \text{docking mode,} \\ C_{PTO}, & \text{power mode.} \end{cases} \tag{13}$$

This is implemented as a logic switch in the control framework as shown in the passive controller block in Fig. 6.

In a two-body point absorber WEC–UUV system, resistive PTO damping governs the degree of dynamic coupling between the float and spar. Increasing C_{PTO} strengthens this interaction, allowing float wave-induced motion to transmit more strongly to the spar. Conversely, setting $C_{PTO} = 0$ allows the spar, and the rigidly attached dock to respond more independently to wave excitation, which may reduce dock excursions during docking operations. This configuration therefore provides a purely passive baseline for docking-mode control.

5.2. Active docking-mode control

Since the PTO provides actuation along a single axis, aligned with the relative motion between the bodies, the active docking-mode control is formulated as a state-feedback problem for the two-body heave dynamics of the float (body 1) and the spar/dock (body 2).

The control-design state vector is

$$x(t) = \begin{bmatrix} z_1(t) & z_2(t) & v_1(t) & v_2(t) \end{bmatrix}^{\top}, \qquad v_i(t) = \dot{z}_i(t), \tag{14}$$

where z_i and v_i denote heave displacement and velocity of body i, respectively.

The linearized heave equations of motion used for control design are written in state-space form as

$$\dot{x}(t) = A(\omega)\,x(t) + B\,u(t) + E(t), \tag{15}$$

where A, B, and E are the system matrix, control input matrix and excitation/disturbance matrix respectively.

The corresponding linearized equation for the two body point absorber in the second-order form is

$$\dot{z} = v, \qquad M_e\,\dot{v} = -K_{hs}\,z - b(\omega)\,v + B_u u(t) + F_{exc}(t), \tag{16}$$

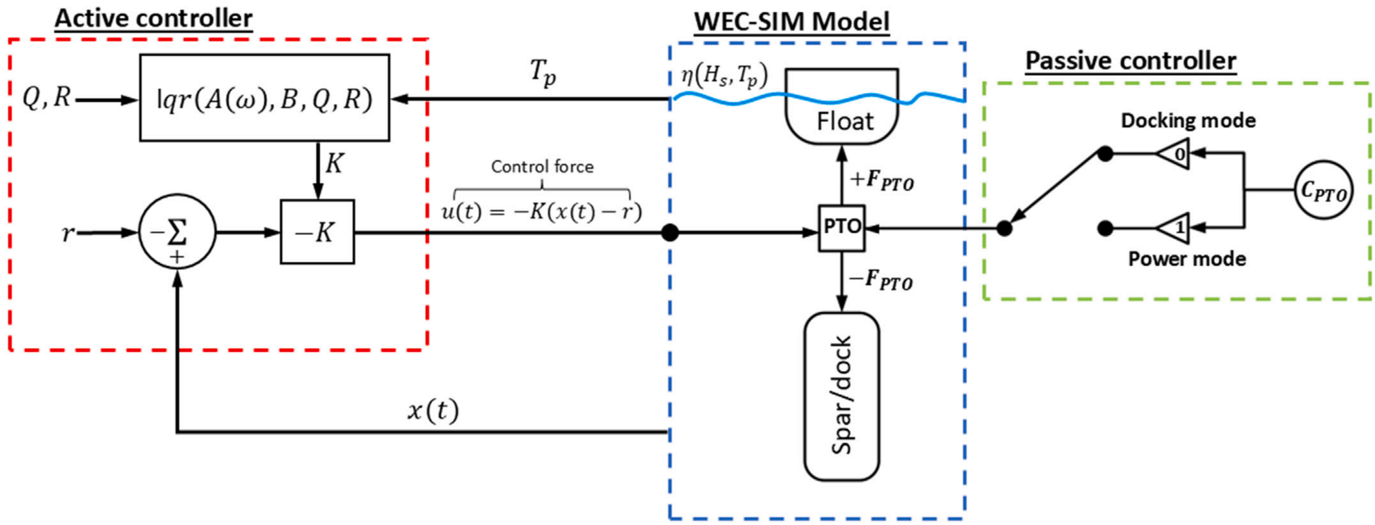

Fig. 6. Numerical implementation of motion control for UUV docking in a two-body point absorber WEC-UUV system.

where the effective inertia matrix is defined as

$$M_e = M + A_\infty, \tag{17}$$

with M the rigid-body mass matrix and A_∞ the infinite-frequency added mass. Hydrostatic restoring is represented by the heave-only matrix K_{hs}. Radiation memory is represented in the control-design model by an equivalent linear damping matrix $b(\omega)$ evaluated at a representative frequency ω (selected from the sea state, e.g., the peak period, $\omega = 2\pi/T_p$).

The control force, $B_u u(t)$ is provided by a single internal PTO acting between the bodies. With, $u(t)$ the control law and the adopted sign convention, B_u is given as,

$$B_u = [1 \ \ -1]^\top \tag{18}$$

The state-space dynamic system matrices are thus given as

$$A(\omega) = \begin{bmatrix} 0_{2\times2} & I_{2\times2} \\ -M_e^{-1}K_{hs} & -M_e^{-1}b(\omega) \end{bmatrix} \in \mathbb{R}^{4\times4}, \qquad B = \begin{bmatrix} 0_{2\times1} \\ M_e^{-1}B_u \end{bmatrix} \in \mathbb{R}^{4\times1}, \tag{19}$$

and the active control law, $u(t)$ is given as;

$$u(t) = -K\,(x(t) - r), \tag{20}$$

where r is the desired reference heave motion requirements for feasible docking and K is the feedback gain. For the two-body heave control model with a single PTO input, $K \in \mathbb{R}^{1\times4}$ contains four coefficients,

$$K = \begin{bmatrix} k_1 & k_2 & k_3 & k_4 \end{bmatrix}, \tag{21}$$

For the numerical implementation in Fig. 6, the feedback control states, $x(t)$ from WEC-SIM are in the global frame thus the control force computed by the control law, Eq. (20) are going to be in the global frame. Since the PTO can only apply force along its actuation axis in the body frame, the desired global heave control force, $u(t)$, must be converted into the corresponding PTO force in the body frame. For a linear PTO aligned with the local heave axis of the body-fixed frame, the PTO unit vector in the body frame is defined as

$$a^b = [0\ 0\ 1]^\top. \tag{22}$$

For a unidirectional point absorber, the yaw and roll motions are assumed negligible, such that $\psi \approx 0$ and $\phi \approx 0$. Under this assumption, the body orientation is described solely by the pitch angle $\theta(t)$, and the rotation matrix reduces to

$$R(t) = \begin{bmatrix} \cos\theta(t) & 0 & \sin\theta(t) \\ 0 & 1 & 0 \\ -\sin\theta(t) & 0 & \cos\theta(t) \end{bmatrix}. \tag{23}$$

The PTO axis expressed in the global frame is therefore

$$a^g(t) = R(t)\,a^b = [\sin\theta(t)\ 0\ \cos\theta(t)]^\top. \tag{24}$$

The scalar PTO force in body frame, f_{PTO} is obtained by projecting the PTO axis, a^b onto the global PTO heave axis a^g

$$f_{\text{PTO}}(t) = \frac{u(t)}{[a^b]^\top a^g(t)} = \frac{u(t)}{\cos\theta(t)}. \tag{25}$$

The generalized PTO load acting on each body consists of a force component and a moment component. In general, this can be written as

$$F_{\text{PTO}}(t) = a^g(t)\,f_{\text{PTO}}(t), \qquad M_{\text{PTO}}(t) = r_b(t) \times F_{\text{PTO}}(t), \tag{26}$$

where $r_b(t)$ is the vector from the body reference point to the PTO application point.

For a two-body point absorber WEC, the translational PTO application point is considered to be at the body's reference point (Beatty et al., 2019; Beringer et al., 2025), so

$$r_b(t) = 0, \qquad M_{\text{PTO}}(t) = [0\ 0\ 0]^\top. \tag{27}$$

Therefore, the generalized PTO force vector applied to each body in docking-mode control, and consistent with Eq. (18), is

$$F_{\text{PTO},1}(t) = \begin{bmatrix} a^g(t)\,f_{\text{PTO}}(t) \\ 0_{3\times1} \end{bmatrix} \in \mathbb{R}^{6\times1}, \qquad F_{\text{PTO},2}(t) = -\begin{bmatrix} a^g(t)\,f_{\text{PTO}}(t) \\ 0_{3\times1} \end{bmatrix} \in \mathbb{R}^{6\times1}. \tag{28}$$

The control gains, K represent the principal control design parameters governing the magnitude and phasing of how the controller input force responds to the instantaneous state, and its deviation, from the reference r. The four gain components k_1–k_4 quantify how the controller allocates feedback control force between displacement and velocity states: gains multiplying displacement states behave as spring-like feedback (units N/m), whereas gains multiplying velocity states behave as damping-like feedback (units N·s/m).

Obtaining suitable feedback gains k_i to achieve the desired docking-mode response is nontrivial. The gains may be selected by direct tuning of a reduced state feedback system, or computed systematically from the linearized state-space model by posing an LQ optimal control problem and solving for the corresponding optimal gain. Both approaches are implemented in this study as described below.

5.2.1. Velocity-proportional feedback controller (VP):

Docking feasibility is primarily governed by spar/dock motion; therefore, the state-feedback structure is reduced to use only the spar/dock heave velocity. This corresponds to selecting $K = \begin{bmatrix} 0 & 0 & 0 & k_4 \end{bmatrix}$ such that the general state-feedback law $u(t) = -K(x(t) - r)$ reduces to

$$u(t) = -k_4\big(v_2(t) - r\big), \tag{29}$$

where r becomes the desired dock velocity for feasible docking. This generates a control force proportional to the deviation of the dock velocity from the reference and provides direct velocity regulation of the spar/dock, driving $v_2(t)$ toward r.

The scalar gain k_4 is treated as a tunable design parameter and selected through a systematic sweep over a prescribed range, with performance evaluated directly using the WEC–UUV numerical model to identify gains that yield the desired spar/dock velocity response. Unlike the PTO damping coefficient used in power-harvesting mode, k_4 is an active feedback proportional gain and therefore does not represent a physical hydrodynamic or mechanical damping parameter.

Following the closed-loop frequency-domain formulation in Coe et al. (2021b), and consistent with the equation of motion in Eq. (16), the heave velocity of body 2 (spar/dock) may be written as

$$v_2(\omega) = \frac{F_{exc,2}(\omega) - u(\omega)}{Z_{i,2}(\omega)}, \tag{30}$$

where $Z_{i,2}(\omega)$ is the hydrodynamic impedance of body 2 and $F_{exc,2}(\omega)$ is the wave-excitation force acting on the spar/dock.

Assuming $r \approx 0$ (for regulating the dock motion to be minimal as possible to be within UUV motion limits), the velocity-proportional control law introduced in Eq. (29), it follows that

$$u = -k_4 v_2. \tag{31}$$

Substituting Eq. (31) into Eq. (30) yields the closed-loop relation

$$v_2(\omega) = \frac{F_{exc,2}(\omega)}{Z_{i,2}(\omega) - k_4}. \tag{32}$$

With the present sign convention in Eq. (18), a stable velocity feedback requires negative values of k_4, since the control force acting on body 2 is $-u = k_4 v_2$, and therefore cancels out excitation on body-2 only when $k_4 < 0$. Consequently, increasing $|k_4|$ increases the effective closed-loop impedance opposing the spar/dock velocity.

In the high-gain limit, when

$$|k_4| \gg |Z_{i,2}(\omega)|, \tag{33}$$

Eq. (32) reduces to

$$v_2(\omega) \approx \frac{F_{exc,2}(\omega)}{-k_4}. \tag{34}$$

Substituting Eq. (34) into Eq. (31) gives

$$u(\omega) = -k_4 v_2(\omega) \approx F_{exc,2}(\omega). \tag{35}$$

Thus, under sufficiently large gain, the control force acting on the spar/dock tends to oppose the excitation force on the spar, such that the net forcing term in Eq. (30), $F_{exc,2}(\omega) - u(\omega)$, approaches zero. Therefore, the velocity-proportional controller acts to approximately cancel the excitation loading on the spar/dock, driving $v_2(\omega)$ toward zero and producing a stabilizing effect that improves docking feasibility through reduced dock motion, consistent with the discussion in Okushemiya et al. (2026a).

Fig. 7, illustrates the performance of the VP controller under regular-wave excitation with $H = 1\,\mathrm{m}$ for different wave periods T_p and gain magnitudes $|k_4|$. Increasing $|k_4|$ consistently reduces the maximum spar/dock velocity, demonstrating the stabilizing effect of the VP feedback and its ability to reduce dock motion.

Across all wave periods, the maximum control force, u, rapidly approaches an approximately constant value as $|k_4|$ increases. In contrast, the net PTO/generator mechanical power continues to improve with increasing $|k_4|$. Since the control-force amplitude remains nearly unchanged, this improvement is primarily associated with the gradual phase shift between the control force, u, and the PTO relative velocity v_r.

The influence of this phase shift can be interpreted using the cycle-averaged harmonic power relation

$$\bar{P}_{\text{net}} = \frac{1}{2}\,\hat{u}\,\hat{v}_r \cos(\Delta\phi_{uv_r}), \tag{36}$$

where $\hat{u}$ and $\hat{v}_r$ denote the amplitudes of u and v_r, respectively, and $\Delta\phi_{uv_r}$ is their phase difference. As $|k_4|$ increases, the phase difference approaches approximately −90°, reducing the magnitude of the average power exchange and therefore improving the net power performance. In some cases the phase becomes slightly less than −90°, allowing the net power to approach or slightly exceed zero.

The results also show that longer wave periods require smaller control forces and yield more favorable net power behavior, whereas shorter periods demand larger actuation. These trends are consistent with the interpretation of k_4 as a nonphysical active feedback gain that regulates dock motion by shaping the closed-loop response, rather than representing a physical PTO damping parameter.

The main advantage of this reduced-order VP controller is its low implementation complexity: it uses a single state for feedback and a single tunable gain. However, because the PTO applies opposing forces on a coupled two-body system, using only the spar/dock velocity for feedback does not explicitly account for how the actuation redistributes response between the float and spar/dock. Consequently, the resulting control action may result in undesired coupled behavior such as excessive motion of the float and may demand large actuation forces for aggressive gains. These limitations motivate the use of a full-state optimal feedback design that computes K optimally using more robust docking and performance objectives.

5.2.2. Linear quadratic full state feedback controller (LQ):

A more robust control objective can be set to regulate spar/dock motion while also taking into account the relative motion that can arise because the internal PTO necessarily applies opposing forces to the two bodies. This is encoded by penalizing spar velocity, relative motion, and an additional penalty on spar displacement to mitigate persistent drift. The control performance output vector is defined as;

$$\begin{aligned} &y(t) = C_y x(t), \qquad y(t) = \begin{bmatrix} z_r(t) & v_r(t) & z_2(t) & v_2(t) \end{bmatrix}^T, \\ &z_r = z_2 - z_1, \quad v_r = v_2 - v_1, \end{aligned} \tag{37}$$

with

$$C_y = \begin{bmatrix} -1 & 1 & 0 & 0 \\ 0 & 0 & -1 & 1 \\ 0 & 1 & 0 & 0 \\ 0 & 0 & 0 & 1 \end{bmatrix}. \tag{38}$$

The infinite-horizon quadratic cost is then posed as

$$\min_{u(\cdot)} \; J = \int_0^\infty \big(y(t)^\top W_y\, y(t) + u(t)^\top R\, u(t) \big)\, dt, \tag{39}$$

where $W_y \succeq 0$ weights docking-relevant variables and $R \succ 0$ penalizes actuation effort. In general, the selection of quadratic weights is a controller design step that involves tunable parameters; however, to make the choice scale-consistent and reproducible, the weights are initialized using Bryson's rule, which normalizes each penalized variable

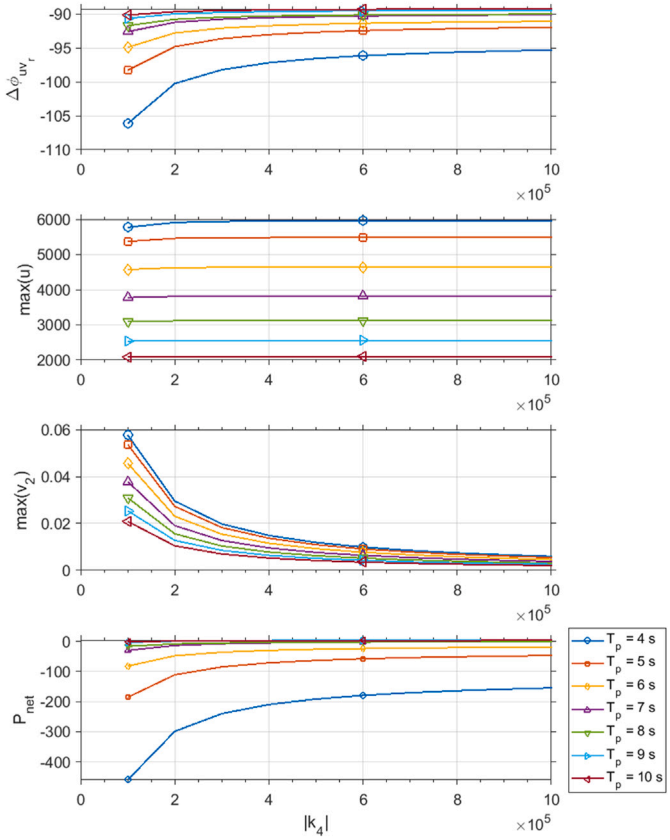

Fig. 7. Behavior of the velocity-proportional (VP) feedback controller as a function of the control gain magnitude $|k_4|$ for regular waves with height $H = 1$ m and periods $T_p = 4$–10 s. The panels show (top to bottom): **phase difference** $\Delta\phi_{uv_r}$ between the control input u and the relative velocity v_r, **maximum control force** $\max(u)$, **maximum heave velocity** $\max(v_2)$ of the spar/dock, and **net mechanical PTO power** P_{net}. Each curve corresponds to a different wave period of the case study WEC-UUV system.

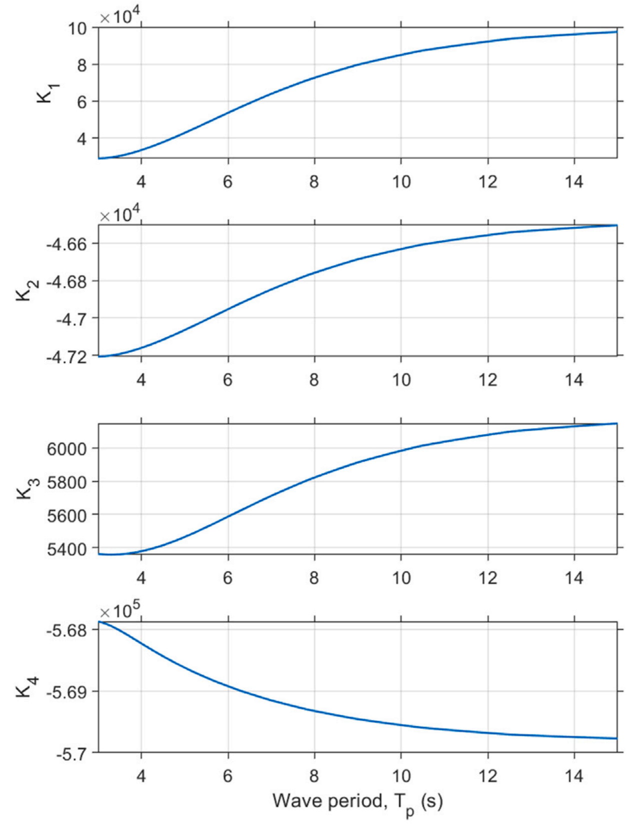

Fig. 8. Variation of the developed LQ control gains with wave period.

by a reference magnitude so that the corresponding contributions to the cost are nondimensional and comparable (Bryson and Ho, 1969). Accordingly, W_y and R are defined as

$$W_y = \operatorname{diag}\left(\frac{w_{zr}}{z_{r,\text{ref}}^2}, \frac{w_{vr}}{v_{r,\text{ref}}^2}, \frac{w_{z2}}{z_{2,\text{ref}}^2}, \frac{w_{v2}}{v_{2,\text{ref}}^2}\right), \qquad R = \frac{w_u}{u_{\text{ref}}^2}, \tag{40}$$

The reference magnitudes are selected to reflect UUV docking feasibility requirements and physically reasonable coupled motion for an internal PTO acting opposite on both bodies: $z_{r,\text{ref}} = 0.75$ m for relative displacement representing the absolute displace of actuator stroke limits, $v_{r,\text{ref}} = 0.5$ m/s for relative velocity, $z_{2,\text{ref}} = 0.5$ m to limit low-frequency spar/dock drift from the control actuation, $v_{2,\text{ref}} = 0.05$ m/s to reflect the primary docking objective of minimal spar/dock relative motion, and $u_{\text{ref}} = 20$ kN as the nominal actuation scale. The dimensionless weights are then chosen to prioritize dock velocity regulation while preventing the controller from achieving this by unrealistically exciting the float; specifically, $w_{v2} = 1.0$ is assigned as the highest priority, $w_{zr} = w_{vr} = 0.5$ provide some penalties on relative motion and relative velocity, $w_{z2} = 0.5$ applies a weak drift penalty, and $w_u = 0.5$ sets the relative penalty on control effort.

The cost may be written in standard LQ form

$$J = \int_0^\infty \left(x^\top Q x + u^\top R u\right) dt, \qquad Q = C_y^\top W_y C_y. \tag{41}$$

where the gain K is obtained by solving the continuous-time algebraic Riccati equation

$$A^\top P + PA - PBR^{-1}B^\top P + Q = 0, \tag{42}$$

and computing

$$K = R^{-1}B^\top P. \tag{43}$$

In implementation, K is computed using standard Riccati solvers (e.g., MATLAB `lqr`).

The achieved control gain values for the system, are presented in Fig. 8, showing their variation with wave period and providing a basis for evaluating how the feedback control gain allocation changes across a wave spectrum band of interest. For the time domain implementation of the control, the gain values are evaluated at the peak period of the irregular wave spectrum as illustrated in Fig. 6.

6. Response of the two-body point absorber WEC–UUV system: heave-only configuration

The response of the two-body point absorber WEC–UUV system is first evaluated under a heave-only configuration without mooring. In this setup, the motion of both bodies is restricted to only vertical translation, enabling characterization and assessment of power–docking performance trade-offs under controlled and uncontrolled response. Wave conditions are simulated using an irregular Pierson–Moskowitz (PM) spectrum, with each realization run for 1200 s.

6.1. Power and docking mode performance trade-offs

The trade-offs between power capture and dock motion are examined by varying the PTO damping from 0 to 150,000 N·s/m under

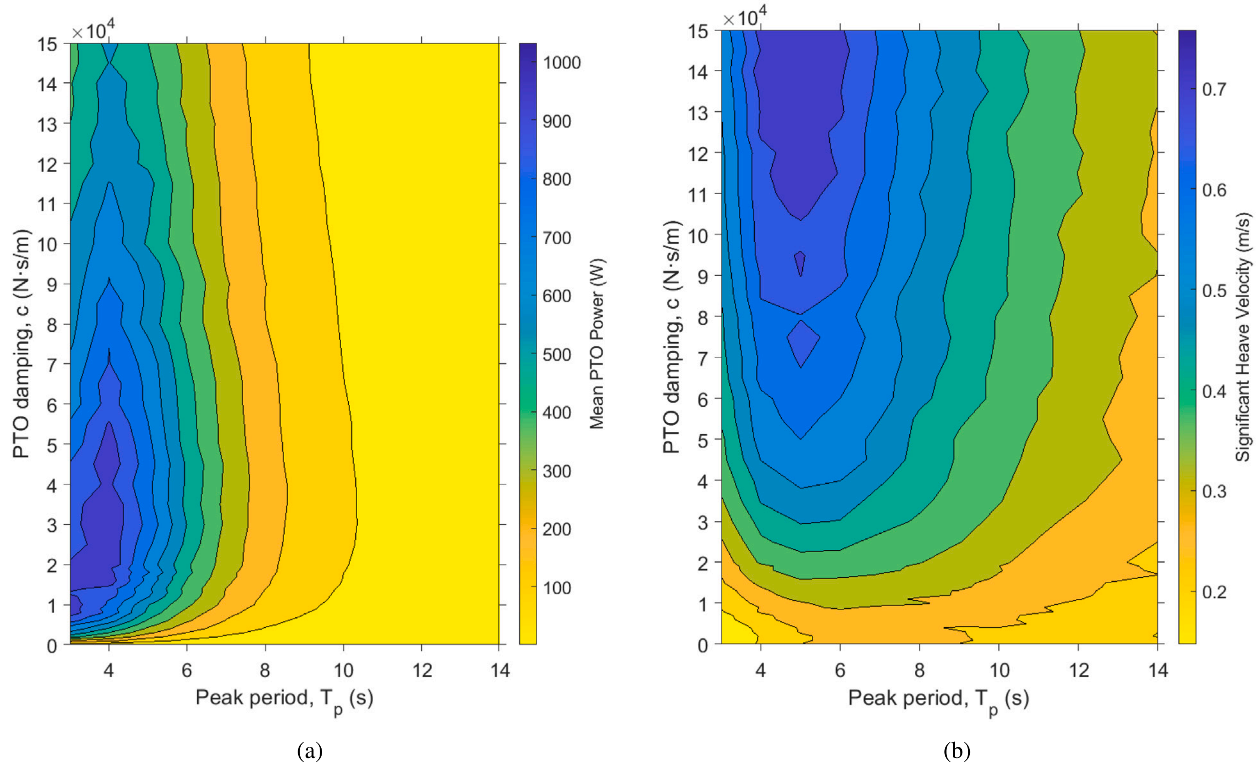

Fig. 9. Influence of PTO damping on power capture and dock motion under irregular wave excitation (PM spectrum, H_s = 1 m, T_p = 3–14 s). (a) Mean mechanical PTO power. (b) Significant dock heave velocity amplitude.

irregular wave excitation modeled using a Pierson–Moskowitz spectrum with significant wave, H_s = 1 m and peak period, T_p = 3 to 14 s. A consistent H_s of 1 m is maintained across all cases to isolate the influence of damping and peak period on system response. Fig. 9 illustrates the resulting mean mechanical PTO power and significant dock heave velocity across peak periods ranging from 3 to 14 s. The significant velocity amplitude is computed as the average of the highest one-third of the response amplitudes.

As shown in Fig. 9(a), the mean PTO power increases from zero damping to an optimal value before decreasing at higher damping levels. The influence of damping is most pronounced at shorter peak periods (T_p = 3–6 s), where distinct power maxima are observed. In contrast, for peak periods beyond approximately $T_p \approx 8$ s, the sensitivity to damping diminishes and the power contours flatten, indicating reduced variation in performance with further increases in damping. This is expected due to the physical size of the WEC and the orbital velocities at higher wave periods. Power performance peaks around $T_p \approx 4$ s and decreases progressively with increasing period, with a marked reduction beyond $T_p \approx 8$ s, as further illustrated in Fig. 10 for a selected damping. Based on these trends, a damping value of 30,000 N·s/m is selected as a representative power-mode damping setting for subsequent analyses, as it represents near-optimal power capture across most of the wave periods while maintaining consistent performance in all simulated sea states. The concentration of energy capture at shorter wave periods is consistent with the dynamic behavior expected for a small-scale point absorber (Majidi et al., 2021). While longer wave periods are prevalent in many open-ocean environments (Ahn et al., 2020), the proposed system is intended for small utility-scale UUV docking and recharging applications, which typically require power on the order of hundreds of watts and motivate the small scale of the device considered in this study. Such small scale systems are suitably deployed in regions characterized by shorter-period sea states (Foteinis, 2022; Okushemiya et al., 2026a), while deployment in

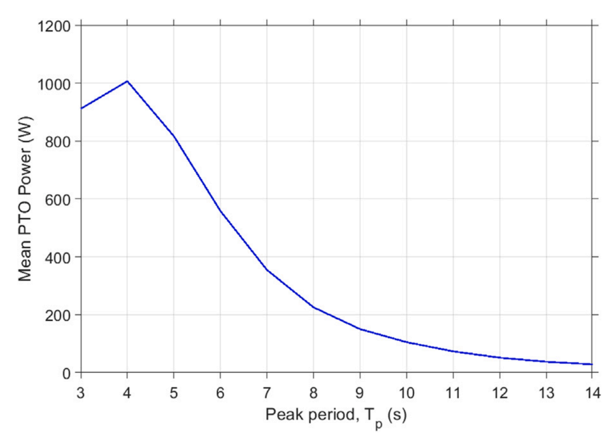

Fig. 10. Variation of mean mechanical PTO power across wave peak periods for the selected representative damping, C_{PTO} = 30,000 N s/m, (PM spectrum H_s = 1 m).

longer-period environments may require dedicated power-maximizing control strategies.

In contrast to the power trends discussed above, Fig. 9(b) confirms that the significant dock heave velocity increases continuously with increasing PTO damping. As the damping approaches and exceeds the optimal value for power generation, the coupling between the float and spar strengthens, resulting in greater transmission of wave-induced motion from the float to the spar/dock. Conversely, near-zero damping allows the spar to move more independently from the float, yielding reduced dock motion levels; however, under higher sea states, even this reduced motion may remain sufficiently large to challenge UUV docking. This trend reinforces the inherent trade-off between power-mode and docking-mode requirements: damping values favorable for

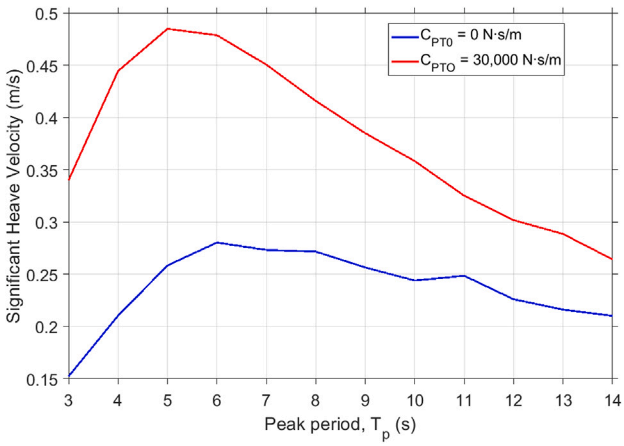

Fig. 11. Variation of significant heave velocity amplitude across wave peak periods, (PM spectrum $H_s = 1$ m).

energy extraction correspond to increased dock motion, thereby reducing docking feasibility (Okushemiya et al., 2026a). The conflicting behavior is clearly illustrated in Fig. 11, where dock motion under the selected power-mode damping (C_{PTO} = 30,000 N·s/m) is substantially higher than in the case of zero PTO damping ($C_{PTO} = 0$), demonstrating the reduction in docking feasibility in power-mode operation and supporting the use of zero PTO damping as a passive docking-mode control strategy.

To characterize the power-mode energy capability of the case-study WEC–UUV system under generalized sea-state conditions, the mean PTO mechanical power is evaluated across a range of sea states using the representative power-mode damping coefficient (C_{PTO} = 30,000 N·s/m). Wave conditions corresponds to irregular waves with significant wave heights in the range H_s = 0.5–5 m, and are simulated using a PM spectrum with peak periods T_p = 3–15 s.

The resulting power matrix, shown in Fig. 12, illustrates the distribution of mean PTO mechanical power over the considered sea states. The electrical power available for UUV recharging will be much lower due to conversion losses across the PTO and power electronics. A methodology to account for these losses and estimate the electrical power is presented in Okushemiya et al. (2026b). The results in the power matrix are therefore intended to illustrate relative power capability for UUV recharging across sea states and do not account for operational limits under extreme sea states.

As shown in Fig. 12, power increases with wave height and is concentrated within shorter peak periods, with maximum values occurring in the range $T_p \approx$ 4–6 s. At longer periods, power decreases progressively despite increasing H_s, consistent with the dynamic behavior expected for a small-scale WEC. The power matrix therefore provides a generalized estimate of the power capability of the 3 m diameter case study device, under moderate to rough sea conditions. It further underscores the importance of aligning the WEC–UUV system scale and design characteristics with the prevailing wave climate at the intended deployment site (Coe et al., 2021a; Zou et al., 2023).

6.2. UUV docking feasibility for power-mode and passive docking-mode control

The docking feasibility quantifies the probability of successful UUV docking at a given sea state and is evaluated using the probabilistic framework introduced in Okushemiya et al. (2026a). It should be noted that this metric reflects compliance with the prescribed UUV velocity limits and does not guarantee 100% docking success. Practical docking additionally depends on the sophistication of UUV control algorithms, as well as sensing and communication with the dock (Okushemiya et al., 2026a). The reported feasibility therefore represents an idealized upper bound on docking success.

For each simulated sea state, the dock velocity time histories $\dot{x}_d^{(k)}(t)$ are evaluated against the corresponding UUV motion limits $\dot{x}_v^{(k)}$ for each degree of freedom k. At each time step t_i, a binary feasibility indicator is defined as

$$f^{(k)}(t_i) = \begin{cases} 1, & \text{if } |\dot{x}_d^{(k)}(t_i)| \le \dot{x}_v^{(k)} \\ 0, & \text{otherwise} \end{cases} \tag{44}$$

The overall instantaneous feasibility is then given by

$$F(t_i) = \prod_{k=1}^{n_{\mathrm{DOF}}} f^{(k)}(t_i), \tag{45}$$

where n_{DOF} denotes the number of motion components considered. The probabilistic docking feasibility for a given sea state is computed as

$$p_{\mathrm{docking}} = \frac{1}{n_t} \sum_{i=1}^{n_t} F(t_i), \tag{46}$$

where n_t is the total number of simulation time steps. The resulting value represents the fraction of time during which the dock motion remains within the prescribed UUV limits. For the heave-only configuration, $n_{\mathrm{DOF}} = 1$, and feasibility is evaluated solely based on the UUV heave velocity limits. The BlueROV2 heave velocity limit is taken as $\dot{x}_v = 0.5$ m/s.

Fig. 13 present the probabilistic UUV docking feasibility for BlueROV2 under power-mode operation (C_{PTO} = 30,000 N·s/m) and passive docking-mode control ($C_{PTO} = 0$), respectively. The feasibility values represent the fraction of time during which the dock heave velocity remains within the BlueROV2 limit of 0.5 m/s.

Under power mode operation (Fig. 13(a)), docking feasibility decreases progressively with increasing significant wave height. While feasibility remains close to unity for slight sea states ($H_s \le 1$ m), a pronounced degradation is observed for moderate-to-rough sea states. For example, at H_s = 2–4 m, docking feasibility drops below 0.6 in several cases, indicating that docking would be feasible less than 60% of the time. This confirms that operating the WEC–UUV system in power mode imposes substantial limitations on docking success in most operational sea states.

In contrast, passive docking-mode control (Fig. 13(b)), achieved by setting $C_{\mathrm{PTO}} = 0$, substantially improves feasibility across the sea-state space. For moderate conditions ($H_s \le 2$ m), docking feasibility remains above 0.9 for most peak periods. Even at higher wave heights (H_s = 3–4 m), feasibility values increase relative to power-mode operation, with many sea states exhibiting improvements of 0.1–0.2 in absolute probability. This improvement directly reflects the reduced dynamic coupling between the float and spar when PTO damping is removed, resulting in lower spar/dock motions. However, passive control does not fully eliminate docking limitations. At $H_s \ge 2$ m, docking feasibility were below unity and decreasing up to 0.5 at high significant wave heights.

The comparison between Figs. 13(a) and 13(b) therefore establishes two critical observations: (i) power-mode operation significantly compromises docking feasibility in even moderate sea states, and (ii) while passive control improves feasibility, it remains insufficient for maintaining high docking feasibility probability across the full operational sea state envelope. These results motivate the need for active docking mode control strategies.

Additionally, under some operating conditions, particularly when UUV docking occurs relatively close to the free surface or under large wave conditions, wave-induced fluid motion may influence docking success. To characterize the magnitude of these disturbances, the water particle velocity at the docking depth was evaluated for the range of sea states considered in this study. Fig. 14, shows the amplitude of the vertical water particle velocity computed under regular wave conditions for a water depth of 70 m, representative of the PacWave

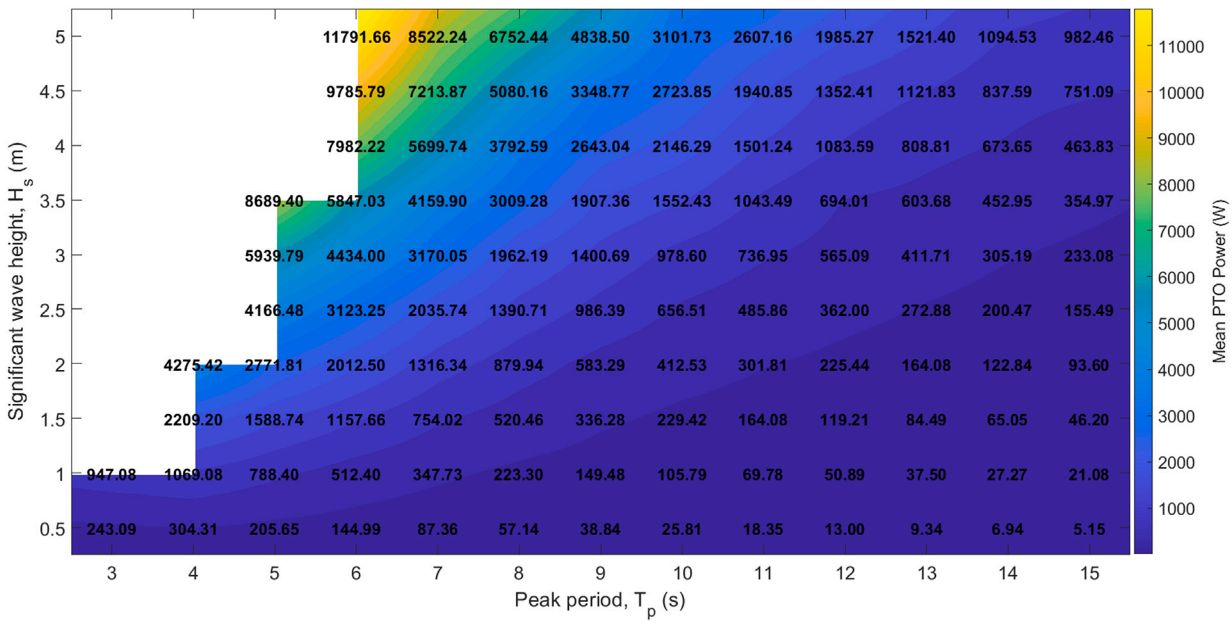

Fig. 12. WEC-UUV PTO mechanical power matrix.

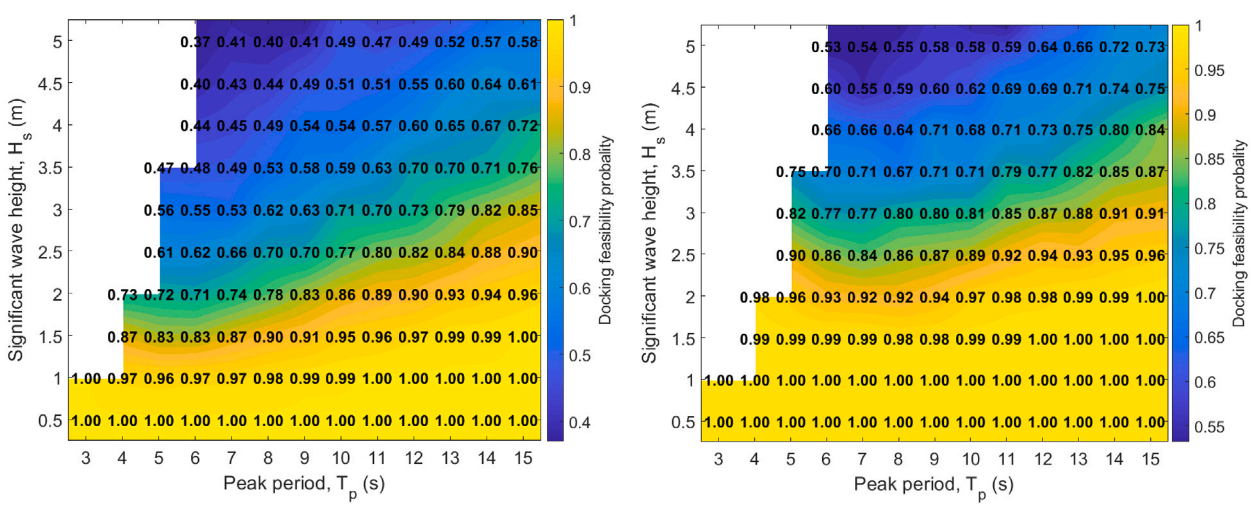

(a)   (b)

Fig. 13. BlueROV2 docking feasibility probabilities for case study WEC-UUV system in; (a) Power mode (C_{PTO} = 30,000 N s/m) (b) Passive control docking mode ($C_{PTO} = 0$ N s/m).

site, and a dock depth of $z = -6.85$ m corresponding to the 3 m LUPA configuration (see Fig. 1). For most of the considered sea states the waves fall within the deep-water regime, where the horizontal and vertical orbital velocity components are of comparable magnitude. The results indicate that water particle velocities at the docking depth can reach significant magnitudes in moderate to rough sea states.

These velocities represent the local fluid motion experienced by a vehicle operating at the docking depth and may induce hydrodynamic forces that influence the vehicle dynamics and motions during the docking approach. As a simplifying assumption, the UUV heave motion may be considered to follow the surrounding vertical water particle velocity. Under this assumption, an alternative docking-mode control objective can be formulated by reshaping the dock motion dynamics such that the dock heave velocity tracks the vertical water particle velocity at the docking depth. Synchronizing the dock heave motion with the assumed vehicle heave response (and ambient wave particle heave motion) reduces the relative heave velocity between the UUV and the dock during the docking maneuver. This effectively allows the UUV control system to allocate its available actuation authority primarily to regulating the surge motion required for approach and alignment with the dock, while the dock control compensates for the wave-induced heave disturbance acting on the vehicle.

Accordingly, two docking-mode control objectives are considered for improved docking feasibility in the following sections: (i) regulation of dock motion to remain minimal and within the prescribed UUV motion limits, and (ii) using a prescribed velocity reference tracking set as the water particle velocity at the docking depth. The performance of

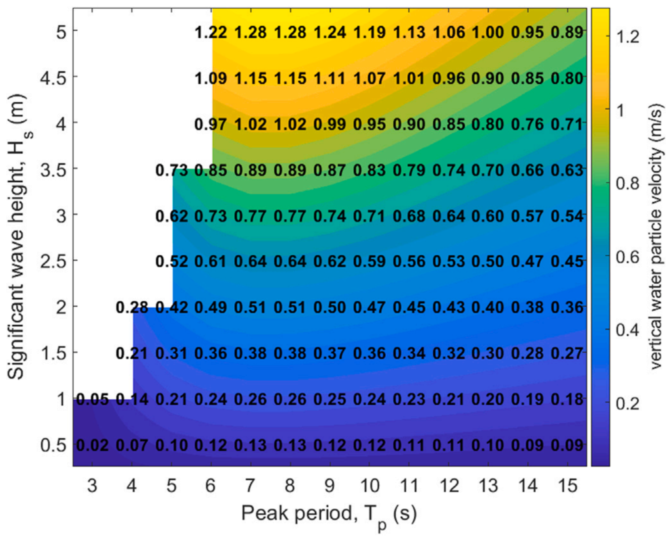

Fig. 14. Amplitude of vertical water particle velocity at the docking depth.

Table 2
Simulated wave conditions.

Simulation ID	Sea state code	H_s (m)	T_p (s)
W1	4	2.5	6
W2	4	2.5	10
W3	6	4.5	8
W4	6	4.5	12

the developed control strategies under these two objectives is evaluated in the subsequent subsections.

6.3. Performance of docking-mode control strategies

The performance of the docking-mode control strategies is evaluated with the primary objective of improving UUV docking feasibility, as defined in Section 6.2. In this context, improving docking feasibility corresponds to regulating dock motion such that its velocity response remains within the limits of the UUV during docking operations. Accordingly, the performance of the WEC-UUV system under power-mode operation (PM), passive docking-mode control (DM), velocity-proportional (VP) active control, and linear quadratic (LQ) active control is evaluated and compared.

A set of four representative sea states is selected to enable a clear and focused evaluation of the control strategies, in conditions of interest identified from the docking feasibility results (Fig. 13). These cases consist of a moderate operational condition (H_s = 2.5 m) and a rough wave extreme condition (H_s = 4.5 m), each evaluated at two peak periods representing shorter- and longer-period excitation. The shorter-period cases are chosen near the dynamically critical response region of the spar (see Fig. 11), while the longer-period cases represent wave periods more consistent with typical ocean wave conditions. The selected cases, denoted as W1–W4, are simulated using irregular waves modeled with a Pierson–Moskowitz spectrum, and are summarized in Table 2.

The control strategies are evaluated using a consistent set of performance metrics, including dock motion response, control force, and associated power, and the resulting UUV docking feasibility. These metrics are presented in the following subsections.

6.3.1. Dock motion response

The dock motion response under the four representative sea states is shown in Fig. 15. Across all cases, a consistent trend is observed in the relative performance of the control modes. Power-mode operation (PM) results in the largest dock motions, with velocity amplitudes approaching 1.0 m/s in W1 and exceeding 1.3 m/s in W3. Passive docking-mode control (DM) reduces the motion relative to PM; however, the reduction remains limited, with velocity amplitudes still on the order of 0.6 m/s in W1–W2 and exceeding 1.0 m/s in W3. These velocity levels remain well above typical UUV operational limits and therefore continue to present challenging docking conditions based on the feasibility definition in Section 6.2.

Based on the docking feasibility framework (Eq. (44) – (46)), the control objective is to regulate the dock motion such that it remains minimal (approaching zero) and within the allowable limits of the UUV.

In contrast to PM and DM, the active control strategies achieve substantial motion reduction across all sea states. The velocity-proportional (VP) controller provides the most significant reduction, limiting velocity amplitudes to approximately 0.02–0.03 m/s across all cases, effectively regulating the dock motion well within UUV limits. The linear quadratic (LQ) controller also reduces dock motion significantly compared to PM and DM; however, residual oscillations remain higher than VP, with velocity amplitudes increasing from approximately 0.05 m/s in W1 to up to 0.3 m/s in W4. While these values represent a substantial improvement over passive approaches, they indicate less aggressive motion regulation compared to VP.

The reduced velocity response achieved by the VP controller implies a higher likelihood of satisfying the docking feasibility condition, whereas the higher residual velocity under LQ suggests comparatively lower, though still improved, feasibility relative to passive approaches. However, this improved motion regulation in VP is achieved at the expense of increased control effort and energy consumption. In contrast, the LQ controller maintains positive net power while still providing substantial motion reduction for improved docking feasibility. This trade-off between motion regulation and power performance is examined in the following subsection.

6.3.2. Control force and power

The PTO control force and corresponding power response under the selected representative sea states are shown in Fig. 16. To achieve the minimal dock motion required for improved docking feasibility, the active control strategies effectively act to counter the wave-induced excitation on the spar such that $F_{\mathrm{exc},2} - F_{\mathrm{PTO}} \approx 0$, thereby reducing the net excitation transmitted to the dock.

Across all sea states, both VP and LQ controllers generate forces of comparable magnitude, generally on the order of 10–20 kN, indicating that similar levels of actuation effort are required. However, the key distinction lies in the phase relationship with the excitation force. The VP controller closely tracks the phase of the excitation, resulting in more effective cancellation and the minimal dock velocities observed in Fig. 15. In contrast, the LQ controller exhibits noticeable phase offsets, leading to less complete cancellation and higher residual motion.

This difference in phase behavior directly influences the power response. The VP controller exhibits predominantly negative power, indicating continuous energy input to regulate motion. In contrast, the LQ controller shows more frequent positive power peaks and reduced negative excursions.

Importantly, the active control forces remain comparable to, and do not exceed, those observed under power-mode (PM) operation, indicating that the required actuation remains within practical PTO limits. Overall, while VP provides the most effective motion regulation, the LQ controller achieves a more favorable balance between motion reduction and energy performance, yielding improved docking feasibility while maintaining positive net power.

6.3.3. Statistical summary

The statistical summary of the docking-mode control performance across the selected sea states is presented in Table 3. The reported

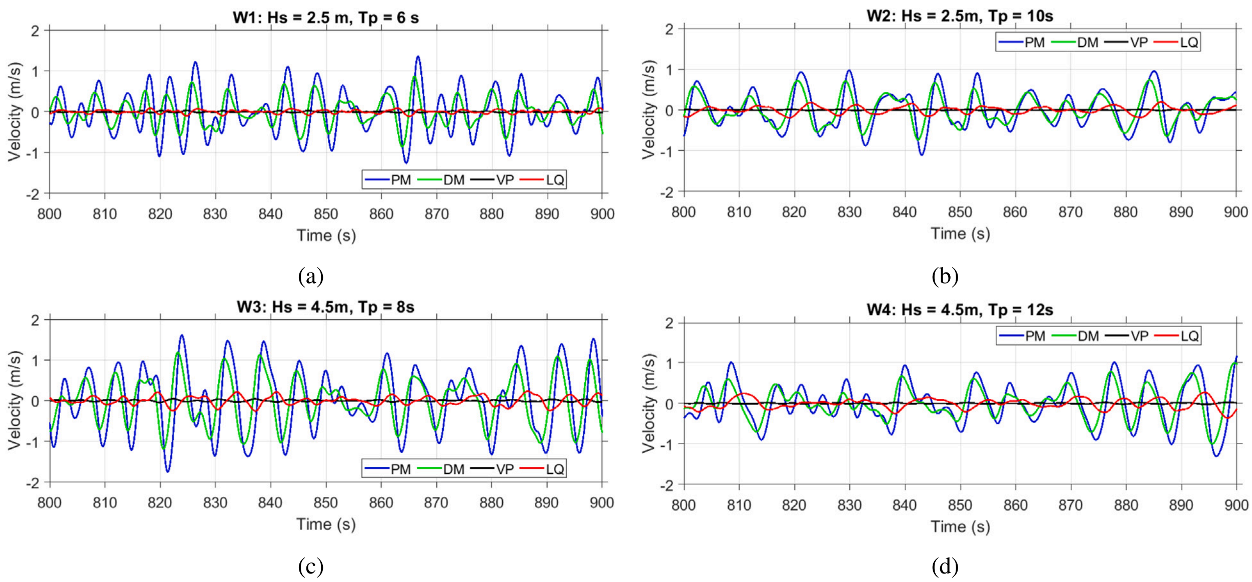

Fig. 15. Spar/Dock motion response under representative sea states and operational control modes.

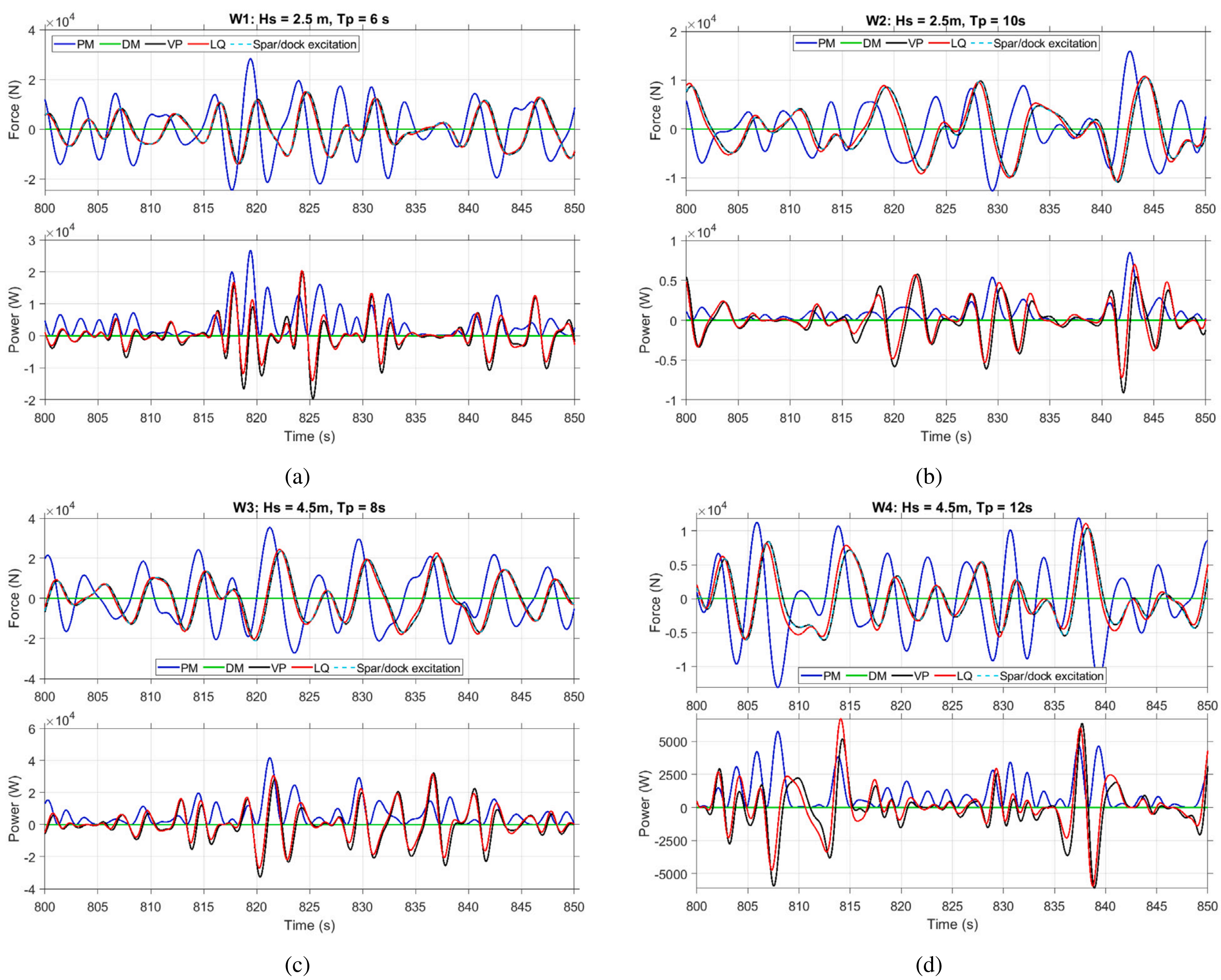

Fig. 16. PTO control force and power response under the selected representative sea states operational control modes.

Table 3
Statistical summary of docking-mode control performance for the selected representative sea states and operational control modes.

Case	Metric	PM	DM	VP	LQ
W1	Dock velocity (m/s)	0.97	0.62	0.02	0.07
	PTO force (kN)	18.11	0.00	11.58	11.49
	Reactive power (W)	0.00	0.00	−2768.25	−2269.38
	Net power (W)	2912.38	0.00	−124.68	423.60
W2	Dock velocity (m/s)	0.77	0.58	0.02	0.14
	PTO force (kN)	8.67	0.00	7.62	7.71
	Reactive power (W)	0.00	0.00	−1166.51	−1016.93
	Net power (W)	662.67	0.00	−34.70	168.64
W3	Dock velocity (m/s)	1.40	1.03	0.03	0.21
	PTO force (kN)	23.21	0.00	17.31	17.45
	Reactive power (W)	0.00	0.00	−5653.04	−4949.42
	Net power (W)	4777.38	0.00	−164.50	908.30
W4	Dock velocity (m/s)	1.08	0.84	0.02	0.28
	PTO force (kN)	12.22	0.00	10.86	11.30
	Reactive power (W)	0.00	0.00	−2509.23	−2292.87
	Net power (W)	1370.56	0.00	−29.38	348.86

motion and PTO force values correspond to significant amplitudes (corresponding to the average of the highest one-third amplitudes), while the reactive and net power values represent time-averaged quantities. The results quantitatively confirm the trends observed in the time-series responses.

Across all sea states, power-mode (PM) and passive docking-mode control (DM) exhibit large dock velocities, exceeding 0.6 m/s in W1–W2 and reaching up to 1.40 m/s in W3, remaining well above typical UUV operational limits. In contrast, the VP controller consistently reduces dock velocity to below 0.03 m/s across all cases, representing over an order-of-magnitude reduction relative to PM. The LQ controller also achieves substantial reduction, with velocities ranging from 0.07 m/s in W1 to 0.28 m/s in W4, indicating improved but less aggressive regulation compared to VP.

The force and power metrics further highlight the trade-off between motion reduction and energy performance. Both VP and LQ require comparable PTO forces (approximately 7–17 kN across all cases), which remain below those observed in power-mode operation (up to 23.21 kN in W3), indicating that active control does not impose increased actuation demand. The power response shows a clear distinction between control strategies. The VP controller consistently exhibits higher reactive power and negative net power (e.g., −124.68 W in W1 and −164.50 W in W3), indicating continuous energy consumption. In contrast, the LQ controller maintains positive net power across all sea states (e.g., 423.60 W in W1 and 908.30 W in W3), corresponding to a reduction of approximately 70–85% relative to PM.

Overall, these results confirm that while the VP controller provides the highest level of motion reduction and thus the greatest improvement in docking feasibility, the LQ controller achieves a more favorable balance between motion regulation and energy performance for practical docking operations.

6.4. Dock motion response under prescribed reference tracking control

As discussed in Section 6.2, wave-induced fluid motion at the docking depth can reach significant magnitudes and may influence the UUV dynamics during docking. Under such conditions, an alternative control objective is to synchronize the dock heave motion with the UUV heave response (or wave-induced water particle vertical orbital velocity), thereby reducing relative motion between the two bodies. This approach may be particularly relevant when docking occurs near the free surface or in moderate to rough sea states where wave-induced velocities are significant.

To demonstrate this capability, the control system is evaluated under a prescribed reference tracking objective, where the reference signal is taken as the vertical water particle velocity (Eq. (9)) at the docking depth (z = -6.85 m). The resulting dock velocity response under VP and LQ control is shown in Fig. 17.

Across all representative sea states (W1–W4), both controllers are able to track the prescribed reference signal with good agreement in both phase and amplitude. The VP controller more closely follows the reference, with near-overlapping time-series responses, while the LQ controller exhibits slight deviations in peak amplitudes and phase. Nevertheless, the overall tracking performance remains strong for both controllers across all cases, indicating that the control system can effectively reshape the dock dynamics to follow a desired motion profile.

It is important to note that the water particle velocity does not necessarily represent the exact UUV heave response, as the vehicle dynamics are also influenced by its inertia, hydrodynamic coefficients, and control system. However, the results demonstrate that the proposed control approach can effectively track a prescribed reference signal.

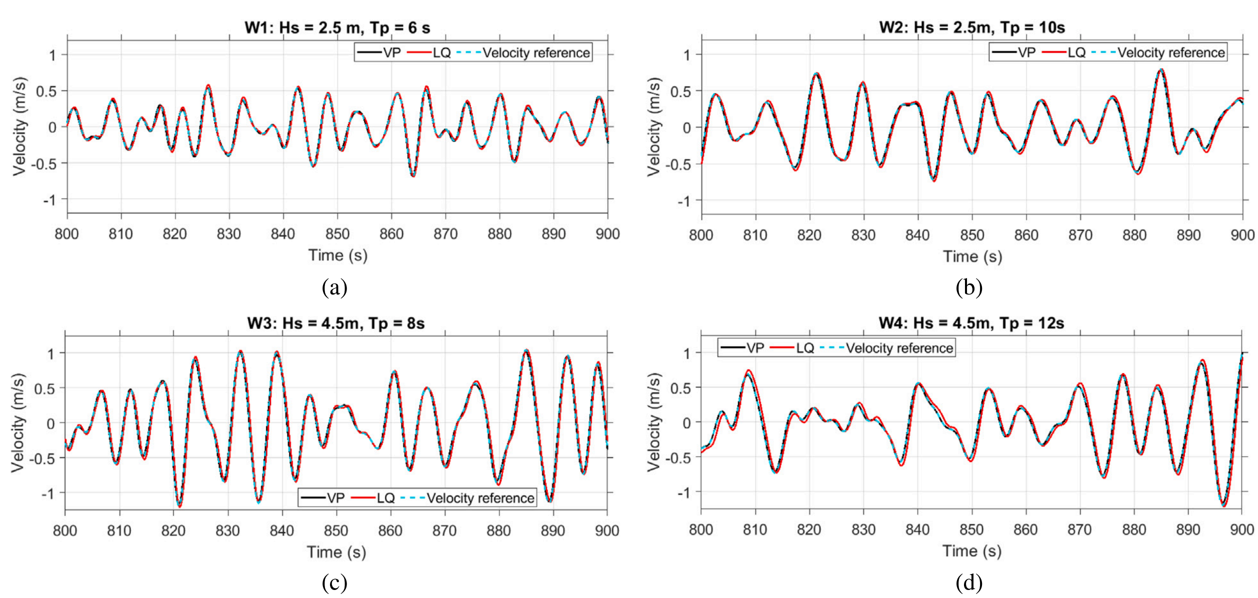

Fig. 17. Spar/dock heave velocity response under prescribed reference tracking control for the selected representative sea states and active control modes.

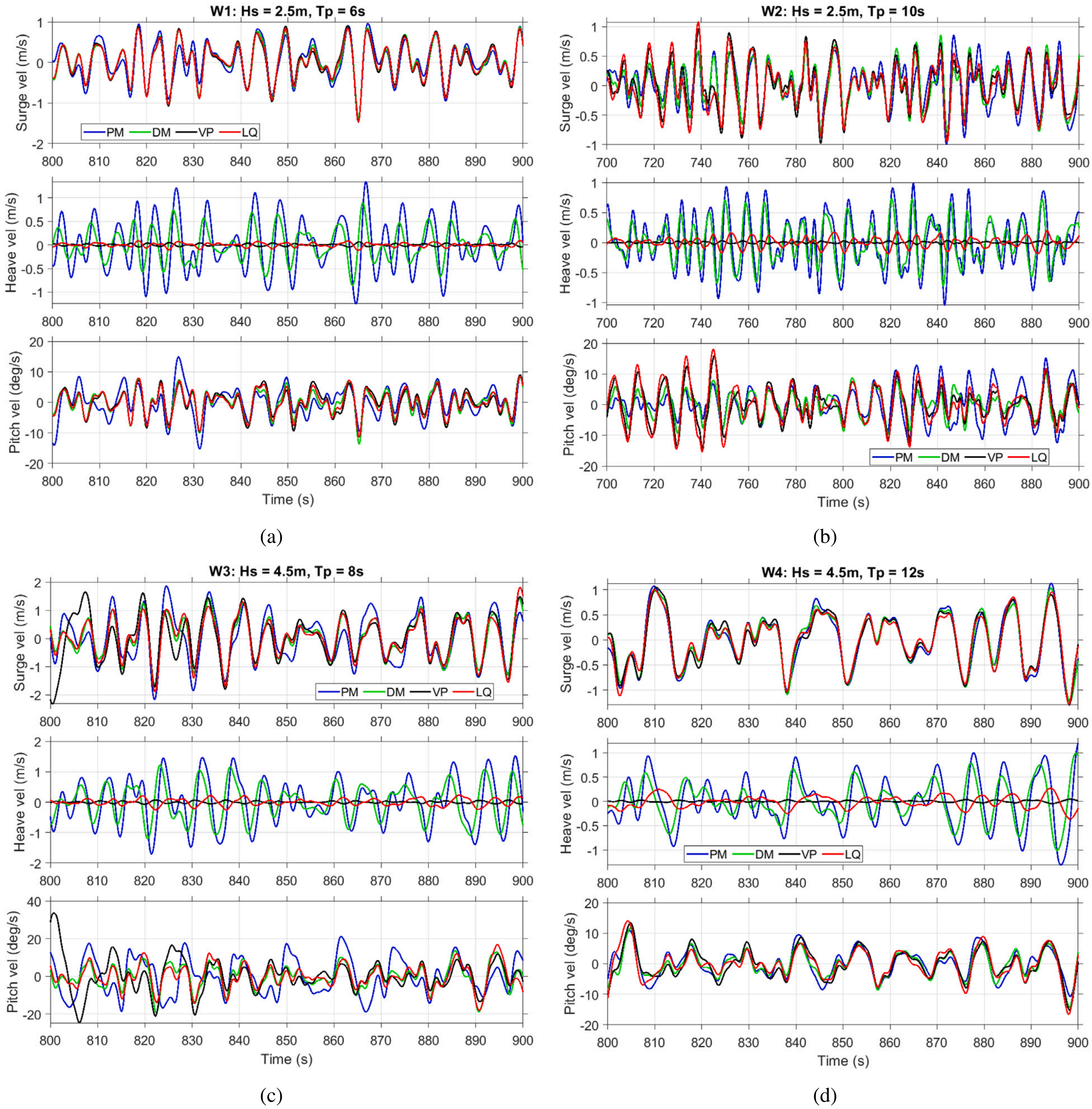

Fig. 18. Spar/dock motion response for the freely floating WEC-UUV system under representative sea states and control modes.

This capability is essential for future scenarios where the dock motion may be synchronized with the estimated or measured UUV motion to further improve docking performance.

7. Response of a freely floating two-body point absorber WEC–UUV system under active heave control

The docking-mode control strategies are applied to a freely floating two-body WEC–UUV system — in which all rigid-body degrees of freedom are unconstrained and no mooring is present. While the control input acts along the heave direction, other rigid-body motions can also influence docking feasibility, as defined in Eq. (45). The system is evaluated under unidirectional irregular wave excitation, using the same representative sea states defined in Table 2. Accordingly, only the surge, heave, and pitch responses are presented, as sway, roll, and yaw are typically negligible for a point absorber WEC under unidirectional wave conditions.

The control objective here is the regulation of dock motion such that it is minimized and maintained within UUV motion limits. The results in Fig. 18, show that this objective is achieved only in heave, with both active controllers significantly suppressing significant heave motion amplitudes from 0.6–1.4 m/s in power mode, PM to 0.03–0.28 m/s across W1–W4 simulated wave cases. However, this reduction does not extend to surge and pitch. While the control action alters the dynamics of these responses through coupled DOF interactions, no clear trend of active motion regulation is observed for surge and pitch. The significant motion amplitudes remain comparable across control modes, with surge velocities remaining on the order of 0.7–1.4 m/s, while pitch velocities range from approximately 7 – 20 deg/s across the simulated wave cases. This indicates that dock motion cannot be actively regulated across all degrees of freedom using the heave-axis translational PTO configuration of the two-body point absorber WEC–UUV system.

8. Discussions

Persistent UUV missions require a reliable at-sea energy source, with WECs offering a promising pathway for enabling docking and recharging offshore. However, the integration of WECs with UUV docking systems introduces competing operational requirements: WEC power-mode operation favors large device motions for energy extraction, whereas docking-mode operation requires minimizing dock motion to remain compatible with UUV limits. Operating across these modes requires a control strategy capable of adjusting the WEC response based on the operational objective. While numerous control strategies have been developed for maximizing wave power extraction for power-mode, control strategies that enable docking-mode operation remain insufficiently studied and understood.

In this study, a feedback control framework is developed to actively regulate dock motion toward a desired reference representative of docking-mode objectives, using the PTO of the WEC as the control input. The results provide insight into the application of motion control for a two-body point absorber WEC-UUV system. The following subsections discuss the resulting system dynamics, the implications of modeling assumptions for physical implementation, and the performance limitations and potential pathways for improvement.

8.1. Control dynamics

In floating point absorber WECs, control strategies are traditionally formulated for power-mode operation, where the objective is to maximize energy extraction by shaping the system response to achieve favorable phase alignment between the excitation force and the relative velocity (Coe et al., 2017). In contrast, docking-mode operation in WEC-UUV systems introduces a fundamentally different objective, in which the motion of the dock, attached to the spar, must be regulated to remain within prescribed limits or to follow a desired motion profile compatible with UUV docking requirements.

For the specific objective of minimizing dock motion, passive docking-mode control can be achieved by reducing the PTO damping toward zero as shown in Fig. 9(b) and Fig. 11. Under this condition, the dynamic coupling between the float and spar is weakened, allowing the spar to respond more independently of the wave-excited float. This decoupling reduces the transmission of wave-induced motion from the float to the spar, resulting in a lower-amplitude spar response. However, while this passive approach provides a reduction in motion relative to power-mode operation, the resulting dock velocities remain non-negligible, particularly under more energetic sea states, and may still exceed typical UUV motion limits, yielding low docking feasibility as shown in Fig. 13. Furthermore, passive control offers limited flexibility in addressing alternative docking objectives, such as enforcing a prescribed motion trajectory.

To achieve further motion regulation, active control is introduced through the PTO. The control law is formulated such that the PTO force is generated from the deviation of the spar/dock motion from a desired reference, thereby driving the response toward docking-mode objectives. In this study, these objectives include minimizing spar/dock motion to remain within UUV operational limits, as well as tracking a prescribed motion, assumed to represent the heave motion of the UUV, to reduce relative heave motion between the UUV and the dock. From the closed-loop relation for the spar/dock velocity (Eq. (32)), the effect of the control gain can be interpreted as modifying the effective impedance of the spar. As the gain magnitude increases, the control force increasingly opposes the wave-excitation force acting on the spar. In the high-gain limit the control input approaches the excitation force, resulting in an approximate cancellation of the net forcing on the spar (Eq. (35)). The control gains therefore do not represent physical system parameters, but rather scale the feedback action used to regulate the spar response toward the desired docking-mode objective in the presence of wave excitation.

Because the PTO applies equal and opposite forces on the float and spar, the control action that opposes the excitation on the spar induces a reaction force on the float that could potentially amplify its motion. However, the full system response (Fig. 19, corresponding to the W3 case for the motion-minimization objective previously presented in Fig. 15(c)) shows that this coupling does not lead to amplification of the float motion under active control, with the float motion response remaining comparable across control modes. This behavior is explained by the force interaction in Fig. 20, where the excitation forces on the float and spar are out of phase, and the control force on the spar acts to oppose the excitation on the spar. Through the PTO coupling and this out-of-phase relationship, the corresponding control force on the float also becomes out of phase with the dominant float excitation, thereby partially counteracting it rather than amplifying it. In addition, the magnitude of the float excitation is significantly larger than that of the spar, which limits the influence of the control input on the float response. Nevertheless, under the docking-mode control objective of minimizing dock motion, the PTO interaction also leads to an increase in relative motion between the bodies, as shown in Fig. 19, since the spar response is suppressed while the float remains primarily wave-driven, resulting in larger PTO stroke requirements that must be accounted for in PTO system design.

The control formulation in this study is not limited to regulating spar/dock motion for underwater docking, but can be extended to alternative objectives by redefining the controlled response variable. For instance, in surface docking and charging applications that may involve unmanned surface vehicles (USVs) and unmanned aerial vehicles(UAVs), the control objective may instead be formulated to regulate or minimize the motion of the surface float.

8.2. Modeling assumptions and implications for physical implementation

The docking-mode control problem considered in this study is formulated as the regulation of dock motion through actuation provided by the PTO. The docking-mode control framework is described by the state vector x, representing the WEC motions, and an output y, corresponding to the dock motion variable of interest, which is regulated toward a desired reference r defining the docking objective. The reference r is prescribed based on the docking requirement, while the control input u is generated by the feedback control law (Eq. (20)) from the deviation between the measured response and the reference. The system states and outputs (x, y) are obtained from the WEC system itself: in a numerical framework, they are directly available from the WEC hydrodynamic model, whereas in a physical system they must be obtained through onboard sensing and state estimation, introducing measurement uncertainty, noise, and delays. Hybrid implementations combining measured data with model-based estimation may also be employed. In the present study, the control framework is implemented using a WEC-Sim numerical plant (as shown in Fig. 6), allowing full access to system states and enabling evaluation and understanding of the control behavior prior to introducing additional complexities associated with physical implementation.

The WEC hydrodynamic model adopted in this study is based on a linear potential flow formulation implemented in the time domain through the Cummins equation, with viscous effects incorporated using a quadratic Morison drag model. The projected area used in the drag formulation includes the contribution of the dock structure to account for its influence on the spar hydrodynamics. Mooring effects are neglected, and the system is analyzed under freely floating conditions. These assumptions allow isolation of the influence of the developed docking-mode control strategies and PTO actuation on spar/dock motion without additional constraints introduced by mooring forces. In

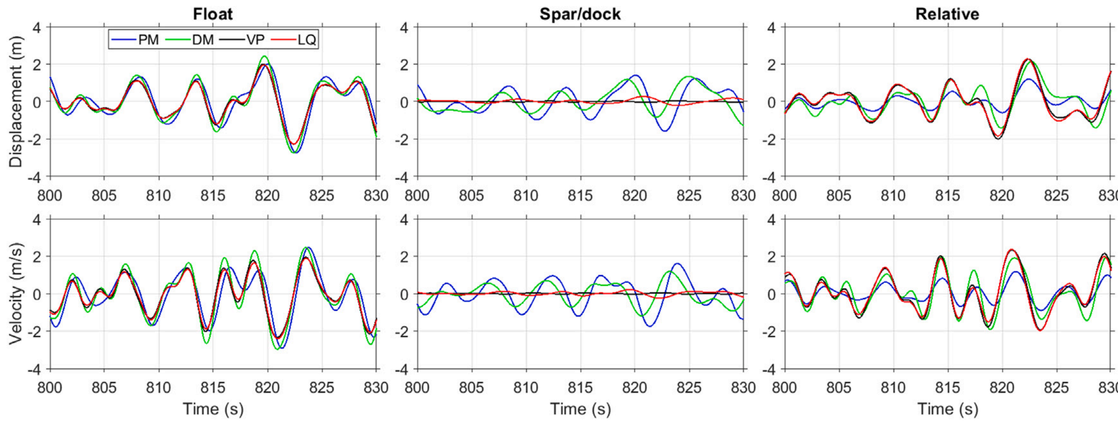

Fig. 19. Full system heave response for the representative sea state (W3: H_s = 4.5 m, T_p = 8 s) under active docking-mode control with dock motion minimization objective.

addition, the present study considers only surge, heave, and pitch response under the assumption of unidirectional wave conditions. Future studies should investigate multidirectional wave environments and the associated sway, roll, and yaw responses to further assess overall docking performance. The WEC numerical modeling in this study is therefore intended to isolate and assess the capability of the docking-mode control strategy, and although the reported performance metrics are subject to modeling assumptions, the results provide a clear understanding of what the control can, and cannot, achieve within the given system configuration.

The PTO control model adopted in this study assumes ideal force actuation, whereby the commanded control input, u is applied directly and instantaneously through the PTO without limitations on force magnitude, rate, or actuator dynamics. This assumption neglects practical constraints such as saturation, bandwidth limits, and delays that may be present in physical PTO systems, and therefore represents the achievable behavior under ideal actuation conditions in regulating dock motion. The control force comparison in Fig. 16 and Table 3 indicates that the forces required under docking-mode operation remain comparable in magnitude to those observed in power-mode operation. This suggests that the proposed docking-mode control strategy does not impose additional actuation demands beyond those for which the PTO would typically be designed.

The implementation of the active docking-mode control in this study assumes perfect state measurement, where the required system states are directly available from the motion response of the WEC numerical model. In practice, these states or WEC motions must be obtained through onboard sensing and state estimation, introducing measurement uncertainty and additional implementation complexity. The sensing requirements depend on the selected docking-mode control strategy: the velocity-proportional (VP) control requires only the spar/dock heave velocity, whereas the linear quadratic (LQ) control requires full-state feedback of the two-body system, necessitating estimation of multiple motion states. A physical implementation of the proposed control framework would therefore involve a sensing-estimation-control loop, where measured responses are processed in real time to compute the PTO control input. While these factors introduce additional practical considerations beyond the present idealized framework, the numerical implementation adopted in this study enables an assessment of the performance and behavior of the developed docking-mode control strategies. Extension of the proposed control framework to a physical WEC–UUV system is therefore identified as a direction for future work.

8.3. Control performance and limitations

The performance of the docking-mode control strategies are evaluated based on their ability to regulate dock motion to improve docking feasibility based on set docking objectives, while accounting for the associated power usage.

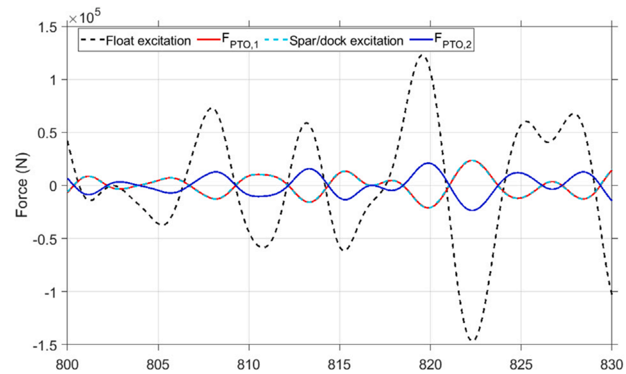

Fig. 20. Wave excitation and PTO control forces for the representative sea state (W3: H_s = 4.5 m, T_p = 8 s) under active docking-mode control with dock motion minimization objective.

The results demonstrate that passive docking control is insufficient to achieve high docking feasibility (Fig. 15), particularly in moderate to rough sea states. This necessitates the use of active control strategies capable of using reactive power to regulate the spar/dock motion within UUV operational limits. Among the active approaches, the velocity-proportional (VP) controller provides the most effective motion regulation, nearly suppressing the dock motion toward zero and closely tracking the prescribed reference motion (Figs. 15 and 17). However, this level of performance is achieved at the expense of increased control effort, resulting in negative net power during docking operations (Table 3). In contrast, the linear quadratic (LQ) controller offers a more balanced trade-off between motion regulation and power usage, reducing dock heave velocities from approximately 0.6–1.4 m/s under power-mode operation to 0.07–0.28 m/s while maintaining positive net PTO power, corresponding to a 70–85% reduction relative to power-mode output (Table 3). In terms of reference tracking, the LQ controller also follows the prescribed motion with good agreement, although with slight phase and amplitude deviations compared to VP. Overall, the performance of the developed active control strategies demonstrates their ability to achieve the defined docking objectives and improve UUV docking conditions, even under energetic sea states.

The difference in performance between the VP and LQ controllers reflects their underlying control formulations and associated trade-offs. The VP controller relies on a single gain acting on the spar velocity, resulting in more direct gain tuning and aggressive motion regulation. In contrast, the LQ controller distributes the control effort across multiple system states, with performance governed by the selection of weighting parameters that balance motion regulation and actuation effort. The performance of the LQ controller is therefore sensitive to the choice of weighting matrices, which define the trade-off between docking feasibility and power consumption. While the weights adopted in this study provide a reasonable balance, systematic tuning or optimization of these parameters could further improve the control performance trade-offs.

Applying active control to the freely floating two-body point absorber WEC–UUV system highlights a fundamental limitation of the proposed approach: actuation through the PTO is restricted to the heave direction and does not provide active control authority over surge and pitch (Fig. 18). This arises from the PTO force being aligned with the heave axis and applied along the centerline, preventing the generation of rotational moments. As a result, while active control can effectively regulate dock heave motion, residual motions in other degrees of freedom may still influence docking conditions. Nevertheless, heave regulation remains significant, as it directly addresses the dominant relative motion during vertical approach and improves overall docking feasibility. In particular, active heave control enables synchronization of the dock and UUV heave motions, allowing the UUV to prioritize its control effort on other degrees of freedom. To further evaluate this synchronization capability, coupled modeling of the WEC-dock and UUV system would be required, enabling coordinated control strategies that account for both WEC and UUV dynamics. Extension of the present framework to such coupled numerical and/or physical implementations is identified as an important direction for future work.

Potential pathways to overcome the control limitations in surge and pitch may be achieved through improved controllability or passive stabilization. One approach is the use of a tethered docking station with an integrated heave plate (Okushemiya et al., 2026b), where the tether connecting the dock to the spar is not rigid enough to transmit rotational motion from the spar to the dock, resulting in a predominantly heave dominated dock response that aligns with the available heave control authority. Another approach could be the use of point absorber configurations employing multiple or spatially offset PTOs, which could enable the generation of control moments and allow active regulation of additional degrees of freedom such as pitch. Passive stabilization strategies, including mooring system design, strakes, and modifications to hydrostatic or geometric properties, may reduce surge and pitch responses and improve docking conditions without direct control action. These approaches are identified as directions for future work. However, any system modifications to improve docking performance should not compromise the energy conversion function of the WEC, as the WEC–UUV system is expected to operate predominantly in power mode, with docking representing an intermittent operational requirement (Okushemiya et al., 2026a).

9. Conclusion

This study presents the development and evaluation of WEC docking-mode motion control strategies for a two-body point absorber WEC–UUV system, where the docking station is rigidly attached to the spar and therefore inherits its motion. The work addresses the conflicting operational requirements in WEC–UUV systems, where power-mode operation favors large spar motions for energy extraction, while docking-mode operation requires the dock motion to remain minimal and compatible with UUV capabilities. Unlike previously studied WEC control, which is formulated for power maximization, this study establishes docking-mode control as a distinct operational framework in which PTO actuation is used to regulate dock motion toward objectives that improve the conditions for successful UUV docking.

The results demonstrate that power-mode (PM) operation and passive docking-mode control (DM) result in unacceptable docking conditions, whereas active control enables effective regulation of dock motion to satisfy defined docking objectives under energetic sea states. For the objective of minimizing dock motion to remain well below UUV motion limits, dock heave velocities on the order of 0.6–1.4 m/s under power-mode operation were reduced to below 0.03 m/s using velocity-proportional (VP) control and to approximately 0.07–0.28 m/s using linear quadratic (LQ) control. In addition, the active controllers effectively regulate the dock motion toward prescribed reference conditions representative of UUV heave motion, thereby reducing relative motion between the UUV and the dock during docking. While VP control achieves the most aggressive regulation, LQ control provides a more balanced trade-off between motion regulation and power usage by maintaining positive net power while still achieving significant motion reduction. These results demonstrate that PTO actuation can be used not only for power extraction in WECs but also for active motion regulation to meet docking-oriented operational requirements. Furthermore, while the control was formulated for underwater docking scenarios, the same framework can be extended to surface docking and charging applications involving unmanned surface or aerial vehicles (USVs and UAVs), where the control objective would be defined to regulate the motion of the surface float.

While the developed control strategies demonstrated strong capability in regulating dock heave motion to satisfy docking objectives, the results also revealed an inherent system-level limitation in the achievable performance. The control action through the PTO was restricted to the heave direction due to its alignment along the centerline of the two-body point absorber, which prevented the generation of control moments and limited active regulation of surge and pitch motions. As a result, residual surge and pitch motions may still present unfavorable conditions for UUV docking. Nevertheless, active heave regulation will significantly improve docking feasibility by reducing the relative heave motion between the UUV and the dock and enabling the UUV control system to prioritize other degrees of freedom. These findings establish that docking-mode control in WEC–UUV systems is governed not only by control design but also by system configuration and controllability. As such, this work provides a foundational understanding of both the capabilities and limitations of PTO-driven motion control, offering practical guidance for the integrated design of control strategies and system architectures required to enable reliable UUV docking in WEC–UUV systems.

Future work will extend the present framework to coupled WEC–UUV system modeling and coordinated control of the WEC and UUV, enabling direct evaluation of motion synchronization between the dock and the UUV during docking operations. Alternative system configurations that improve controllability, including tethered dock configurations, multi-PTO configurations, and passive stabilization strategies, will also be investigated. Experimental validation and real-time implementation of docking-mode control in physical WEC–UUV systems remain important directions for future work.

CRediT authorship contribution statement

David Okushemiya: Writing – original draft, Methodology, Investigation, Formal analysis, Data curation, Conceptualization. **Bryson Robertson:** Writing – review & editing, Supervision, Funding acquisition. **Junhui Lou:** Writing – review & editing. **Solomon C. Yim:** Writing – review & editing.

Declaration of competing interest

The authors declare that they have no known competing financial interests or personal relationships that could have appeared to influence the work reported in this paper.

Acknowledgments

This research is supported by the U.S. Department of Energy's Office of Energy Efficiency and Renewable Energy (EERE) under FOA2234 Topic Area 1:Marine Energy Foundational Research and Testing Infrastructure, DE-EE0009449.

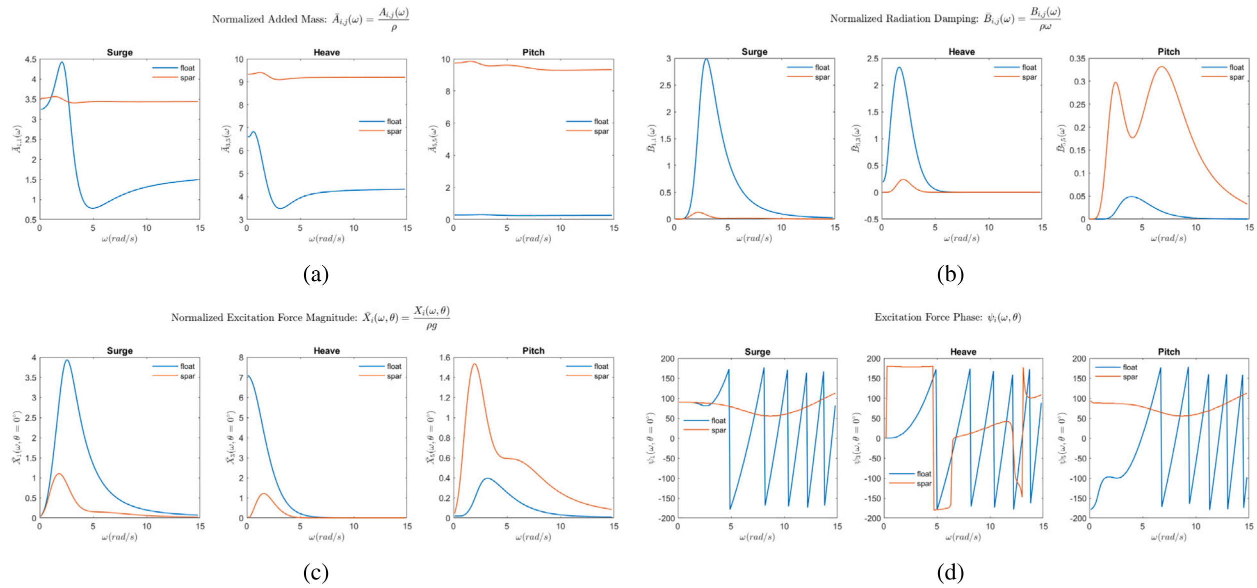

Fig. 21. The frequency dependent hydrodynamic coefficients of the float and spar from WAMIT for the case study LUPA WEC in surge, heave and pitch. (a) Normalized added mass coefficients. ρ is the water density and $\rho = 1000$ kg/m3 is used in this WEC-Sim modeling. (b) Normalized radiation damping coefficients. (c) Normalized excitation force magnitudes. (d) Excitation force phases in degrees.

Appendix

The hydrodynamic parameters of the float and spar of this case study 3:1 scale LUPA (3 m float diameter) WEC calculated from WAMIT and plotted directly using WEC-Sim "Bemio" feature are shown in Fig. 21.

The normalized hydrostatic restoring matrices for the float and spar are given by

$$\frac{K_{hs,1}}{\rho g} = \begin{bmatrix} 0 & 0 & 0 & 0 & 0 & 0 \\ 0 & 0 & 0 & 0 & 0 & 0 \\ 0 & 0 & 7.1075 & -0.0056 & -0.0190 & 0 \\ 0 & 0 & -0.0056 & -0.0065 & 0 & 0 \\ 0 & 0 & -0.0190 & 0 & -0.0060 & 0 \\ 0 & 0 & 0 & 0 & 0 & 0 \end{bmatrix}, \tag{47}$$

$$\frac{K_{hs,2}}{\rho g} = \begin{bmatrix} 0 & 0 & 0 & 0 & 0 & 0 \\ 0 & 0 & 0 & 0 & 0 & 0 \\ 0 & 0 & 0.0727 & 0 & -0.0026 & 0 \\ 0 & 0 & 0 & 6.4702 & 0.0001 & 0 \\ 0 & 0 & -0.0026 & 0.0001 & 6.4705 & 0 \\ 0 & 0 & 0 & 0 & 0 & 0 \end{bmatrix}. \tag{48}$$

References

Abdelkhalik, O., Zou, S., 2019. Control of small two-body heaving wave energy converters for ocean measurement applications. Renew. Energy 132, 587–595. http://dx.doi.org/10.1016/j.renene.2018.08.004.

Ahn, S., Haas, K.A., Neary, V.S., 2020. Wave energy resource characterization and assessment for coastal waters of the United States. Appl. Energy 267, 114922. http://dx.doi.org/10.1016/j.apenergy.2020.114922.

Åström, K.J., Murray, R., 2021. Feedback Systems: an Introduction for Scientists and Engineers. Princeton University Press.

Bacelli, G., 2014. Optimal Control of Wave Energy Converters (Ph.D. thesis). National University of Ireland Maynooth, URL: https://mural.maynoothuniversity.ie/id/eprint/6753/.

Beatty, S.J., Bocking, B., Bubbar, K., Buckham, B.J., Wild, P., 2019. Experimental and numerical comparisons of self-reacting point absorber wave energy converters in irregular waves. Ocean Eng. 173, 716–731. http://dx.doi.org/10.1016/j.oceaneng.2019.01.034.

Beringer, C., Bosma, B., Robertson, B., 2025. A numerical and experimental study of wave energy converter number of bodies and degrees of freedom. Renew. Energy 125089. http://dx.doi.org/10.1016/j.renene.2025.125089.

BlueRobotics, 2023. BlueROV2 specification. URL: https://bluerobotics.com/store/rov/bluerov2/. (Accessed 17 April 2023).

Bryson, A.E., Ho, Y.C., 1969. Applied Optimal Control: Optimization, Estimation, and Control. Blaisdell Publishing Company, Waltham, MA.

Chen, M., Vivekanandan, R., Rusch, C.J., Okushemiya, D., Manalang, D., Robertson, B., Hollinger, G.A., 2024. A unified simulation framework for wave energy powered underwater vehicle docking and charging. Appl. Energy 361, 122877. http://dx.doi.org/10.1016/j.apenergy.2024.122877.

Coe, R.G., Ahn, S., Neary, V.S., Kobos, P.H., Bacelli, G., 2021a. Maybe less is more: Considering capacity factor, saturation, variability, and filtering effects of wave energy devices. Appl. Energy 291, 116763. http://dx.doi.org/10.1016/j.apenergy.2021.116763, URL: https://www.sciencedirect.com/science/article/pii/S0306261921002701.

Coe, R.G., Bacelli, G., Forbush, D., 2021b. A practical approach to wave energy modeling and control. Renew. Sustain. Energy Rev. 142, 110791. http://dx.doi.org/10.1016/j.rser.2021.110791.

Coe, R.G., Bacelli, G., Wilson, D.G., Abdelkhalik, O., Korde, U.A., Robinett III, R.D., 2017. A comparison of control strategies for wave energy converters. Int. J. Mar. Energy 20, 45–63. http://dx.doi.org/10.1016/j.ijome.2017.11.001.

de Andrés, A., Guanche, R., Armesto, J., del Jesus, F., Vidal, C., Losada, I., 2013. Time domain model for a two-body heave converter: Model and applications. Ocean Eng. 72, 116–123. http://dx.doi.org/10.1016/j.oceaneng.2013.06.019.

Department of Energy, 2019. Wave Energy Resource Assessment and Technology Development Program: 2018 Annual Report. Technical Report, U.S. Department of Energy, URL: https://www.energy.gov/sites/prod/files/2019/09/f66/73355-3.pdf.

Driscol, B.P., Gish, L.A., Coe, R.G., 2021. A scoping study to determine the location-specific WEC threshold size for wave-powered AUV recharging. IEEE J. Ocean. Eng. 46 (1), 1–10. http://dx.doi.org/10.1109/JOE.2020.2973032.

Falnes, J., Kurniawan, A., 2020. Ocean waves and oscillating systems: Linear interactions including wave-energy extraction, second ed. In: Cambridge Ocean Technology Series, vol. 8, Cambridge University Press, United Kingdom, http://dx.doi.org/10.1017/9781108674812.

Fletcher, B., Martin, S., Flores, G., Jones, A., Nguyen, A., Brown, M.H., Moore, D.L., 2017. From the lab to the ocean: Characterizing the critical docking parameters for a free floating dock with a REMUS 600. In: OCEANS 2017 - Anchorage. pp. 1–7.

Forbush, D.D., Bacelli, G., Spencer, S.J., Coe, R.G., 2020. A self-tuning WEC controller for changing sea states. IFAC-PapersOnLine 53 (2), 12307–12312. http://dx.doi.org/10.1016/j.ifacol.2020.12.1185, 21st IFAC World Congress.

Foteinis, S., 2022. Wave energy converters in low energy seas: Current state and opportunities. Renew. Sustain. Energy Rev. 162, 112448. http://dx.doi.org/10.1016/j.rser.2022.112448.

Freeman, M.C., O'Neil, R., Garavelli, L., Hellin, D., Klure, J., 2022. Case study on the novel permitting and authorization of PacWave south, a US grid-connected wave energy test facility: Development, challenges, and insights. Energy Policy 168, 113141. http://dx.doi.org/10.1016/j.enpol.2022.113141.

Gao, T., Zhang, Y., Tezdogan, T., 2025. Noncausal explicit model predictive control of wave energy converters. Ocean Eng. 338, 121999. http://dx.doi.org/10.1016/j.oceaneng.2025.121999.

Guo, J., Liu, M., Pan, X., Zhu, J., Liu, J., Xu, H., Peng, Z., Cui, J.H., 2024a. Moored underwater docking system for resident UUVs with acoustic guidance: Design and experiment. Ocean Eng. 294, 116802. http://dx.doi.org/10.1016/j.oceaneng.2024.116802.

Guo, J., Tan, H., Liu, J., Feng, W., Peng, Z., Liu, Y., Cui, J.H., 2024b. Numerical simulation and analysis of UUV docking with a seabed Moored floating dock. Ocean Eng. 313, 119528. http://dx.doi.org/10.1016/j.oceaneng.2024.119528.

Hagen, P.E., Størkersen, N., Marthinsen, B.E., Sten, G., Vestgård, K., 2008. Rapid environmental assessment with autonomous underwater vehicles — examples from HUGIN operations. J. Mar. Syst. 69 (1), 137–145. http://dx.doi.org/10.1016/j.jmarsys.2007.02.011, Maritime Rapid Environmental Assessment.

Hasan, K., Ahmad, S., Liaf, A.F., Karimi, M., Ahmed, T., Shawon, M.A., Mekhilef, S., 2024. Oceanic challenges to technological solutions: A review of autonomous underwater vehicle path technologies in biomimicry, control, navigation, and sensing. IEEE Access 12, 46202–46231. http://dx.doi.org/10.1109/ACCESS.2024.3380458.

Jin, S., Greaves, D., 2021. Wave energy in the UK: Status review and future perspectives. Renew. Sustain. Energy Rev. 143, 110932. http://dx.doi.org/10.1016/j.rser.2021.110932.

Kassem, A.M., Besheer, A.H., Abdelaziz, A.Y., 2015. A linear quadratic Gaussian approach for power transfer maximization of a point absorber wave energy converter. Electr. Power Compon. Syst. 43 (8–10), 1173–1181. http://dx.doi.org/10.1080/15325008.2015.1010048.

Korde, U.A., 2002. Latching control of deep water wave energy devices using an active reference. Ocean Eng. 29 (11), 1343–1355. http://dx.doi.org/10.1016/S0029-8018(01)00093-2.

Li, D., Sharma, S., Borthwick, A.G., Huang, H., Dong, X., Li, Y., Shi, H., 2023. Experimental study of a floating two-body wave energy converter. Renew. Energy 218, 119351. http://dx.doi.org/10.1016/j.renene.2023.119351.

Li, H., Wu, X., Zhang, Z., Tan, X., Pan, Y., Dai, C., Luo, D., Ahmed, A., Xu, Y., 2022. An extended-range wave-powered autonomous underwater vehicle applied to underwater wireless sensor networks. IScience 25 (8), 104738. http://dx.doi.org/10.1016/j.isci.2022.104738.

Lin, M., Lin, R., Yang, C., Li, D., Zhang, Z., Zhao, Y., Ding, W., 2022. Docking to an underwater suspended charging station: Systematic design and experimental tests. Ocean Eng. 249, 110766. http://dx.doi.org/10.1016/j.oceaneng.2022.110766.

Liu, J., Yu, F., He, B., Soares, C.G., 2024. A review of underwater docking and charging technology for autonomous vehicles. Ocean Eng. 297, 117154. http://dx.doi.org/10.1016/j.oceaneng.2024.117154.

Lou, J., Okushemiya, D., Robertson, B., 2025. Wave distortion methodology for experimental mixed-scale testing of underwater vehicle docking. In: International Conference on Offshore Mechanics and Arctic Engineering. Volume 3: Ocean Engineering; Polar and Arctic Sciences and Technology, http://dx.doi.org/10.1115/OMAE2025-156599, V003T06A041.

Majidi, A., Bingölbali, B., Akpınar, A., Iglesias, G., Jafali, H., 2021. Downscaling wave energy converters for optimum performance in low-energy seas. Renew. Energy 168, 705–722. http://dx.doi.org/10.1016/j.renene.2020.12.092.

Meng, L., Lin, Y., Gu, H., Bai, G., Su, T.C., 2019. Study on dynamic characteristics analysis of underwater dynamic docking device. Ocean Eng. 180, 1–9. http://dx.doi.org/10.1016/j.oceaneng.2019.03.033.

Mundon, T.R., Rosenberg, B.J., Murrillo, M., 2024. An integrated wave energy recharging system for autonomous underwater vehicles. In: Offshore Technology Conference. In: OTC Offshore Technology Conference, http://dx.doi.org/10.4043/35198-MS, D011S006R002.

Nemoto, Y., Takino, M., Tsukamoto, S., Asai, T., 2022. Numerical study of a point absorber wave energy converter with tuned variable inerter. Ocean Eng. 257, 111696. http://dx.doi.org/10.1016/j.oceaneng.2022.111696.

Okushemiya, D., Robertson, B., Rusch, C.J., 2026a. Performance and feasibility assessment of a wave energy converter with underwater vehicle docking and charging. Appl. Energy 409, 127453. http://dx.doi.org/10.1016/j.apenergy.2026.127453.

Okushemiya, D., Rusch, C.J., Robertson, B., Zhang, Z., 2025. Wave energy conversion for persistent AUV capability: A case study of the field deployed tigerray WEC-auv system. In: OCEANS 2025 - Great Lakes. pp. 01–10. http://dx.doi.org/10.23919/OCEANS59106.2025.11245068.

Okushemiya, D., Rusch, C.J., Robertson, B., Zhang, Z., 2026b. Model validation and improved PTO modeling of a field-deployed wave energy converter with tethered heave plate. Appl. Ocean Res. 166, 104921. http://dx.doi.org/10.1016/j.apor.2026.104921.

Podder, T., Sibenac, M., Bellingham, J., 2004. AUV docking system for sustainable science missions. In: IEEE International Conference on Robotics and Automation, 2004. Proceedings. ICRA '04. 2004, vol. 5, pp. 4478–4484 Vol.5. http://dx.doi.org/10.1109/ROBOT.2004.1302423.

Rahimi, A., Rezaei, S., Parvizian, J., Mansourzadeh, S., Lund, J., Hssini, R., Düster, A., 2022. Numerical and experimental study of the hydrodynamic coefficients and power absorption of a two-body point absorber wave energy converter. Renew. Energy 201, 181–193. http://dx.doi.org/10.1016/j.renene.2022.10.103.

Robertson, B., Bailey, H., Clancy, D., Ortiz, J., Buckham, B., 2016. Influence of wave resource assessment methodology on wave energy production estimates. Renew. Energy 86, 1145–1160. http://dx.doi.org/10.1016/j.renene.2015.09.020.

Robertson, B., Bailey, H., Leary, M., Buckham, B., 2021a. A methodology for architecture agnostic and time flexible representations of wave energy converter performance. Appl. Energy 287, 116588. http://dx.doi.org/10.1016/j.apenergy.2021.116588.

Robertson, B., Dunkle, G., Gadasi, J., Garcia-Medina, G., Yang, Z., 2021b. Holistic marine energy resource assessments: A wave and offshore wind perspective of metocean conditions. Renew. Energy 170, 286–301. http://dx.doi.org/10.1016/j.renene.2021.01.136.

Ruehl, K., Keester, A., Forbush, D., Grasberger, J., Husain, S., Shabara, M.A., Leon, J., Ogden, D., 2025. WEC-sim v7.0.0. http://dx.doi.org/10.5281/zenodo.16950906.

Rusch, C.J., Hammagren, E., Prudell, J., Zhang, Z., Thomson, J., 2026. Development and operation of a 100 w wave energy converter for persistent ocean observation. Sci. Rep. http://dx.doi.org/10.1038/s41598-026-55823-z.

Sarda, E.I., Dhanak, M.R., 2019. Launch and recovery of an autonomous underwater vehicle from a station-keeping unmanned surface vehicle. IEEE J. Ocean. Eng. 44 (2), 290–299. http://dx.doi.org/10.1109/JOE.2018.2867988.

Scruggs, J., Lattanzio, S., Taflanidis, A., Cassidy, I., 2013. Optimal causal control of a wave energy converter in a random sea. Appl. Ocean Res. 42, 1–15. http://dx.doi.org/10.1016/j.apor.2013.03.004.

Song, J., Abdelkhalik, O., Robinett, R., Bacelli, G., Wilson, D., Korde, U., 2016. Multi-resonant feedback control of heave wave energy converters. Ocean Eng. 127, 269–278. http://dx.doi.org/10.1016/j.oceaneng.2016.09.046.

Song, Z., Marburg, A., Manalang, D., 2020. Resident subsea robotic systems: A review. Marine Technol. Soc. J. 54 (5), 21–31. http://dx.doi.org/10.4031/MTSJ.54.5.4.

Stokey, R., Allen, B., Austin, T., Goldsborough, R., Forrester, N., Purcell, M., von Alt, C., 2001. Enabling technologies for REMUS docking: an integral component of an autonomous ocean-sampling network. IEEE J. Ocean. Eng. 26 (4), 487–497. http://dx.doi.org/10.1109/48.972082.

Stokey, R., Purcell, M., Forrester, N., Austin, T., Goldsborough, R., Allen, B., von Alt, C., 1997. A docking system for REMUS, an autonomous underwater vehicle. In: Oceans '97. MTS/IEEE Conference Proceedings, vol. 2, pp. 1132–1136 vol.2. http://dx.doi.org/10.1109/OCEANS.1997.624151.

WAMIT, Version 7.2 User Manual. Massachusetts Institute of Technology, Cambridge, MA, USA, URL: https://www.wamit.com/manualupdate/v72_manual.pdf.

Wu, S., Liu, Y., Qin, J., 2021. Experimental analyses of two-body wave energy converters with hydraulic power take-off damping in regular and irregular waves. IET Renew. Power Gener. 15 (14), 3165–3175. http://dx.doi.org/10.1049/rpg2.12218.

Xu, Q., Li, Y., Yu, Y.H., Ding, B., Jiang, Z., Lin, Z., Cazzolato, B., 2019. Experimental and numerical investigations of a two-body floating-point absorber wave energy converter in regular waves. J. Fluids Struct. 91, 102613. http://dx.doi.org/10.1016/j.jfluidstructs.2019.03.006.

Yazdani, A., Sammut, K., Yakimenko, O., Lammas, A., 2020. A survey of underwater docking guidance systems. Robot. Auton. Syst. 124, 103382. http://dx.doi.org/10.1016/j.robot.2019.103382.

Zeng, Z., Lian, L., Sammut, K., He, F., Tang, Y., Lammas, A., 2015. A survey on path planning for persistent autonomy of autonomous underwater vehicles. Ocean Eng. 110, 303–313. http://dx.doi.org/10.1016/j.oceaneng.2015.10.007.

Zeng, F., Wang, T., 2023. In-situ wave energy harvesting for unmanned marine devices: A review. Ocean Eng. 285, 115376. http://dx.doi.org/10.1016/j.oceaneng.2023.115376.

Zhan, S., Na, J., Li, G., Wang, B., 2020. Adaptive model predictive control of wave energy converters. IEEE Trans. Sustain. Energy 11 (1), 229–238. http://dx.doi.org/10.1109/TSTE.2018.2889767.

Zhang, Y., Liu, Q., Gao, F., Zhou, S., Zhang, W., Chen, W., 2024. Design and modeling of wave energy converter glider (WEC-glider) with simulation validation in wave tank experiments. Appl. Energy 364, 123175. http://dx.doi.org/10.1016/j.apenergy.2024.123175.

Zhang, Y., Wen, Y., Han, X., Zhang, W., Gao, F., Chen, W., 2023. Gyroscopic wave energy converter with a self-accelerating rotor in WEC-glider. Ocean Eng. 273, 113819. http://dx.doi.org/10.1016/j.oceaneng.2023.113819.

Zhang, M., Yu, S.R., Zhao, G.W., Dai, S.S., He, F., Yuan, Z.M., 2024. Model predictive control of wave energy converters. Ocean Eng. 301, 117430. http://dx.doi.org/10.1016/j.oceaneng.2024.117430.

Zheng, R., Tan, H., Lv, Z., Xu, H., Yu, Z., 2024. Dynamic characteristics of deep-sea single-point mooring levitation docking system. Ocean Eng. 301, 117536. http://dx.doi.org/10.1016/j.oceaneng.2024.117536.

Zou, S., Abdelkhalik, O., 2020. Time-varying linear quadratic Gaussian optimal control for three-degree-of-freedom wave energy converters. Renew. Energy 149, 217–225. http://dx.doi.org/10.1016/j.renene.2019.12.054.

Zou, S., Abdelkhalik, O., Robinett, R., Bacelli, G., Wilson, D., 2017. Optimal control of wave energy converters. Renew. Energy 103, 217–225. http://dx.doi.org/10.1016/j.renene.2016.11.036.

Zou, S., Robertson, B., Paudel, S., 2023. Geospatial analysis of technical U.S. wave net power potential. Renew. Energy 210, 725–736. http://dx.doi.org/10.1016/j.renene.2023.04.060, URL: https://www.sciencedirect.com/science/article/pii/S0960148123005104.